Marine Geology 378 (2016) 312–332

Contents lists available at ScienceDirect

Marine Geology

journal homepage: www.elsevier.com/locate/margo

Influence of bottom currents on the sedimentary processes at the western tip of the Gulf of Corinth, Greece

A. Beckers [a,b,*], C. Beck [b], A. Hubert-Ferrari [a], E. Tripsanas [c], C. Crouzet [b], D. Sakellariou [d], G. Papatheodorou [e], M. De Batist [f]

[a] Department of Geography, University of Liège, Liège B-4000, Belgium
[b] ISTerre, CNRS UMR 5275, University Savoie Mont Blanc, Le Bourget du Lac F-73376, France
[c] Shell U.K. Limited, Specialist Geology Team, Aberdeen AB12 3FY, UK
[d] Institute of Oceanography, Hellenic Center for Marine Research, Anavyssos GR-19013, Greece
[e] Laboratory of Marine Geology and Physical Oceanography, Department of Geology, University of Patras, Patras 26500, Greece
[f] Renard Centre of Marine Geology, University of Gent, Gent B-9000, Belgium

ARTICLE INFO

Article history:
Received 10 May 2015
Received in revised form 31 January 2016
Accepted 3 March 2016
Available online 4 March 2016

Keywords:
Sedimentary drift
Muddy contourite
Furrow
Magnetic fabric
Magnetic anisotropy
Holocene
Mediterranean Sea

ABSTRACT

We investigated the sedimentary processes that were active during the Holocene in the Gulf of Corinth, using high-resolution seismic reflection profiles and gravity cores. Seismic reflection data clearly show the presence of shallow-water sediment drifts at the western end of the Gulf, close to the Rion sill that links the Gulf to the Ionian Sea. Short cores indicate that drifts are composed of homogenous bioturbated mud in their upper part. The drift deposits flank a wide central area where the seafloor is eroded and where pre-Holocene deposits locally outcrop. The seafloor morphology in this area is marked by furrows oriented in different directions and by a depression attributed to the action of bottom-currents. The magnetic fabric of sediment samples from the drift, shelves, sub-basins and from the basin floor shows a significant anisotropy and a similar orientation of K_{max} axes along core. The largest anisotropy ($P = 1.043 \pm 0.007$) is observed in the drift and is interpreted as resulting from the action of bottom currents. The similar orientation of K_{max} axes in the other cores, collected from areas east of the drifts, suggests that bottom currents also affect sediment deposition in the rest of the study area, even if seismic profiles and core analyses demonstrate that gravitational processes such as submarine landslides and turbidity currents exert the main control on sediment transport and deposition. Average K_{max} axes for four cores were reoriented using the declination of the characteristic remanent magnetization. K_{max} axes show variable orientations relatively to the slope of the seafloor, between along-slope and roughly parallel to the contour lines.

1. Introduction

In the marine realm, water circulation plays an important role in the transfer of heat, sediments, nutrients and pollutants, and also transfer of dissolved salt. In deep-water environments (>2000 m), water-mass movements are largely driven by the global thermohaline circulation. Water circulation along the seafloor takes place in so-called bottom currents and is often responsible for the development of typical depositional and erosional reliefs, contouritic drifts and channels. Contourite depositional systems (CDSs) have been described since the 1960s in many places around the world, mainly in the deep ocean, but also in shallower settings (<300 m) as well as in lakes (e. g. Verdicchio and Trincardi, 2008a,b; Rebesco et al., 2014). In shallow-water environments, the water circulation is controlled by other processes such as winds, tides, and continental fresh water outflows, besides thermohaline mechanisms. Contourite systems at the outlet of semi-enclosed basins such as fjords, gulfs, or seas, such as the Baltic and the Black Sea, the Sea of Marmara, and the Strait of Gibraltar (Kuscu et al., 2002; Sivkov et al., 2002; Hernandez-Molina et al., 2003) are common features, due the strengthening of the flows at narrow passages. This study focuses on a shallow-water area in which bottom currents interact with gravity-driven processes, at the western tip of the Gulf of Corinth, in the Mediterranean Sea (Fig. 1A). The objective is to unravel the

* Corresponding author at: Department of Geography, University of Liège, Liège B-4000, Belgium.
E-mail addresses: beckersarnaud@gmail.com (A. Beckers), christian.beck@univ-savoie.fr (C. Beck), aurelia.ferrari@ulg.ac.be (A. Hubert-Ferrari), etripsan@gmail.com (E. Tripsanas), christian.crouzet@univ-smb.fr (C. Crouzet), sakell@hcmr.gr (D. Sakellariou), gpapathe@upatras.gr (G. Papatheodorou), Marc.DeBatist@UGent.be (M. De Batist).

http://dx.doi.org/10.1016/j.margeo.2016.03.001
0025-3227/

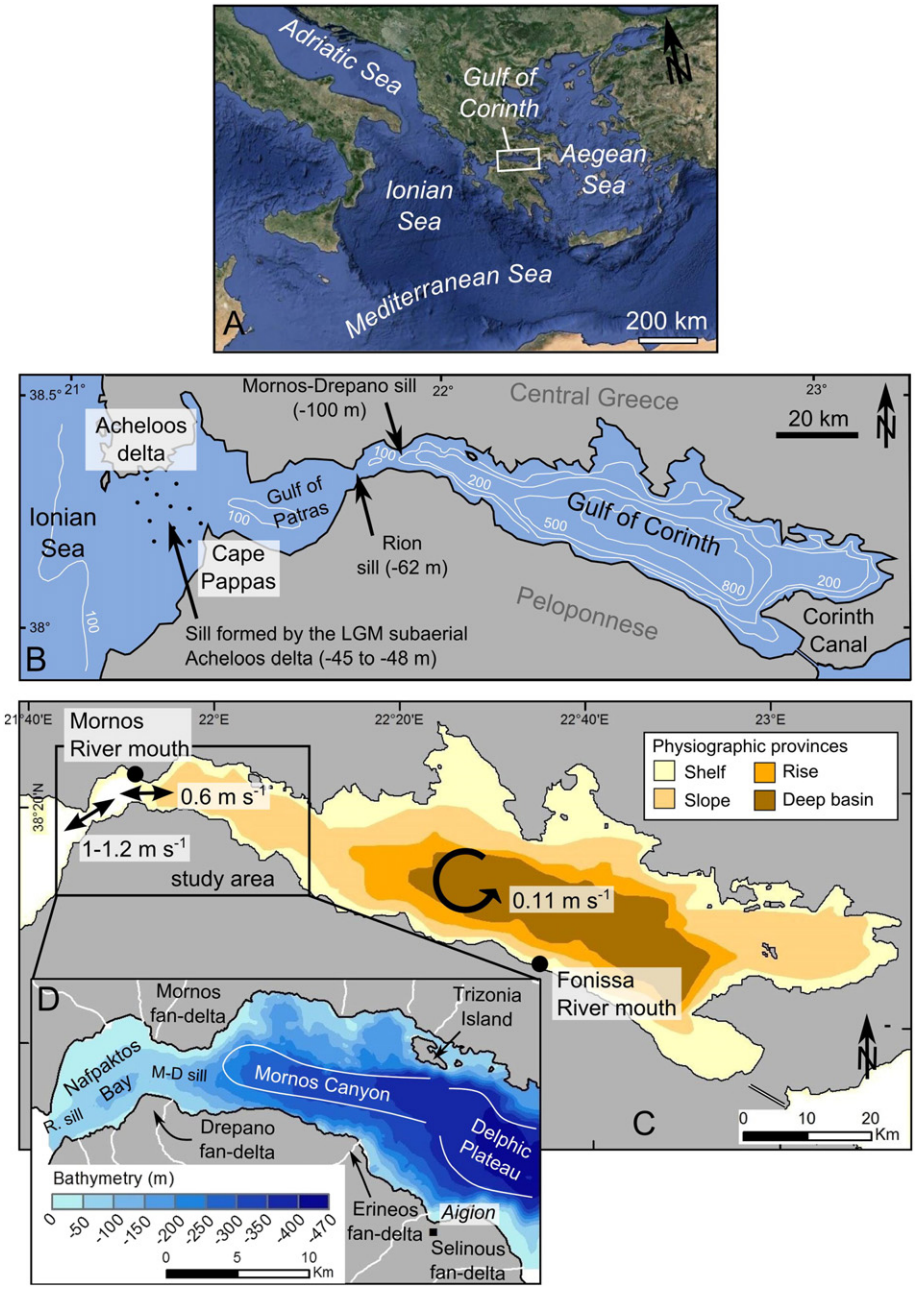

Fig. 1. Location, morphology, physiographic provinces and available current data for the Gulf of Corinth. A) Location of the Gulf of Corinth within the Mediterranean Sea. B) Map view of the connections between the Gulf of Corinth, the Gulf of Patras, and the Ionian Sea. C) Physiographic provinces according to Poulos et al. (1996) and current data from the literature (1–1.2 m s^{-1} from Hadjitheodorou et al., 1992 in Fourniotis and Horsch, 2010; 0.6 m s^{-1} from Lascaratos et al., 1989 and 0.11 m s^{-1} according to modeling in Lascaratos et al., 1989). D) Bathymetry of the study area and location of the sites presented in this study. R. sill = Rion sill, M.–D. sill = Mornos–Drepano sill.

influence of bottom currents in relation to the other sedimentary processes. The analysis is based on high resolution seismic profiles and short gravity cores. The main morphosedimentary features and the Holocene deposits lateral distribution in the area are presented. An attempt is made to investigate the influence of bottom currents based on a combination of sediment magnetic fabric and grain-size data.

2. Regional setting

2.1. Physiographic setting

The Gulf of Corinth is a 120 km long, up to 30 km wide, and 867 m deep water body connected to the Ionian Sea, in Greece (Fig. 1A and B). The Gulf separates continental Greece to the north from the Peloponnese to the south. Today, the Gulf is connected at its western tip to the Mediterranean Sea through three shallow sills (Fig. 1B). The 62 m deep Rion sill and the 100 m deep Mornos–Drepano sill connect the Gulf of Corinth to the 138 m deep Gulf of Patras (Perissoratis et al., 2000). Farther to the west, the Gulf of Patras joins the Ionian Sea through a third, 45–48 m deep, sill that lies along the line Acheloos delta to Cape Pappas (Piper et al., 1988). This sill is covered by 5–7 m of Holocene sediments (G. Ferentinos, pers. comm.). This regional physiographic setting implies that the Gulf of Corinth was disconnected from the World Ocean during the Late Quaternary lowstands. This has been proved by coring for the last glacial period (Collier et al., 2000; Moretti et al., 2004; Campos et al., 2013a). Since 1893, the Gulf of Corinth is also artificially connected to the Aegean Sea at its eastern tip through the Corinthian canal. In the Gulf of Corinth itself, different physiographic

provinces have been defined (Fig. 1C). A deep basin stretches in the central part of the Gulf and is surrounded by shelves, continental slopes and continental rise (Fig. 1C; Poulos et al., 1996).

This study focuses on a 35 km long sector at the entrance of the Gulf of Corinth, between the Rion Straits to the west and the Selinous River delta to the east (Fig. 1D). Morphologically, this area can be divided in different zones. To the west, the Nafpaktos Bay is a 8 km long, 115 m deep depression that lies between the Rion straits and the Mornos–Drepano sill (Fig. 1D). The latter is formed by the coalescence of the Mornos River delta, to the north, and the smaller Drepano River delta, to the south. East of the Mornos–Drepano sill, the Gulf deepens and forms the W–E striking, 14 km long Mornos Canyon dipping toward the east (Fig. 1D). The northern flank of the canyon is a tectonic scarp while the southern flank encompasses fault scarps and Gilbert-type deltas (Beckers et al., 2015). East of the Trizonia Island meridian, the deep gulf widens and forms the so called Delphic Plateau, at a depth of about −400 m (Fig. 1D; Heezen et al., 1966).

2.2. Geological setting

The Gulf of Corinth sedimentary basin results from the tectonic subsidence in the Corinth Rift. The rifting was initiated ~5 Ma ago, to the south and east of the present gulf, and then shifted northward to the present gulf area probably at the beginning of the Quaternary (Ori, 1989; Ford et al., 2009). The Gulf of Corinth basin is affected by numerous active faults, mainly located on the southern coastline, but also offshore and along the northern coast (e. g. Stefatos et al., 2002; Bell et al., 2008, 2009; Taylor et al., 2011; Charalampakis et al., 2014; Beckers et al., 2015). The fault network controls the overall morphology of the Gulf described in the previous section at the scale of the whole Gulf as well as at the scale of the study area, at its western tip.

2.3. Oceanography

Published current data from the Gulf of Corinth are few, so that the understanding of water circulation is still incomplete. Strong currents have been measured at the entrance of the Gulf of Corinth, over the Rion sill area (~1.0 m s^{-1}) and over the Mornos–Drepano sill, located ca. 9 km further to the east (0.6 m s^{-1}) (Fig. 1C, Hellenic Hydrographie Service, 1984 in Lascaratos et al., 1989). Modeling of the marine currents in the Gulf of Patras for different boundary conditions suggests that currents at the entrance of the Gulf of Corinth are generally controlled by tides, and occasionally by winds (Fourniotis and Horsch, 2012). Modeled rising tide-induced currents are unidirectional in winter, but in summer, a cold-water bottom-current flows from the Gulf of Corinth to the Gulf of Patras, while a warmer current flows in an upper layer in the opposite direction (Fourniotis and Horsch, 2012). In the central gulf near-bed current meter data and water-surface temperature analysis suggest that the velocity of the currents is very low (<8 cm s^{-1}, Poulos et al., 1996) and that a counterclockwise gyre is centered in this area (Lascaratos et al., 1989) (Fig. 1C). The Gulf of Corinth waters show a thermal stratification in summer. The upper layer, from 0 to ~100 m shows a strong thermal gradient from 21 to 26 °C at the surface to ~13 °C just below the thermocline, while below 100 m, the temperature is uniformly at 13 °C. In winter, the convection homogenizes the temperature profile around 13 °C (Lascaratos et al., 1989; Poulos et al., 1996).

2.4. Sedimentological setting

Sediment characteristics and sedimentary processes in the Gulf of Corinth have been studied for half a century by seismic reflection profiling and gravity coring (Heezen et al., 1966; Ferentinos et al., 1988; Piper et al., 1988, 1990; Papatheodorou and Ferentinos, 1997; Perissoratis et al., 2000; Lykousis et al., 2007a, 2009). South of the Gulf, in the Peloponnese, an extended drainage network cuts through a thick cover of uplifted synrift deposits, delivering large amounts of sediments to the Gulf. Those rivers develop giant Gilbert-type deltas along the southern coast, while deltas on the northern coast are smaller and thinner (Piper et al., 1990; Ford et al., 2013). Slopes are highly unstable (Ferentinos et al., 1988; Lykousis et al., 2009). During the last centuries, submarine landslides have been triggered by earthquakes but others also occurred aseismically, most often during the rainy season because of sediment overloading near river mouths (Galanopoulos et al., 1964; Heezen et al., 1966). Numerous debris-flow deposits and mass-transport deposits (MTDs) have accumulated at the foot of the delta foresets and form wide coalescing delta fans (Ferentinos et al., 1988), named "continental rise" by Poulos et al. (1996) (Fig. 1C). Turbidity currents feed the abyssal plain, alternating with hemipelagic sedimentation (Heezen et al., 1966; Papatheodorou et al., 2003; Moretti et al., 2004; Lykousis et al., 2007a; Van Welden, 2007; Campos et al., 2013a). At the western tip of the Gulf, in the Mornos Canyon and the Delphic Plateau (Fig. 1D), a similar alternation between turbidites and hemipelagites has been documented by Heezen et al. (1966) and Lykousis et al. (2007b) from gravity cores. In the Nafpaktos Bay, Piper et al. (1990) and Lykousis (1990) describe an area where seafloor erosion currently occurs, but no deposit associated to the action of bottom currents has been described so far in this area, or in the Gulf of Corinth in general.

A seismic stratigraphy has been established for the ~3 km thick sedimentary infill in the deep basin (e.g. Bell et al., 2009; Taylor et al., 2011). This stratigraphy is based on the inferred alternations between marine and non-marine conditions in the Gulf through the Quaternary. Based on that, Bell et al. (2009) proposed an age of 1–2 Ma for the initiation of the sedimentation in the present Gulf. At the western tip of the Gulf, a seismic stratigraphy has been established by Beckers et al. (2015) and concerns the last 130 ka. This stratigraphic framework has been developed based on the high-resolution seismic data used in this study. In shallow-water areas (<200 m), the stratigraphy is based on two unconformities interpreted as the MIS 5 and MIS 1 transgression surfaces. For the deeper Mornos Canyon and the Delphic Plateau areas (Fig. 1D), reflectors corresponding to these two transgressions have been identified by correlation with other studies in the western and central gulf (Bell et al., 2008, 2009). Different sedimentary units tracing the last post-glacial sea level rise have also been highlighted from higher-resolution seismic data at the western tip of the Gulf (Lykousis et al., 2009). These authors describe that in the low-gradient prodelta areas, one unit of transgressive systems tract is overlain by a prodelta wedge of the late Holocene highstand systems tract. Ages of 18–6 ka BP and 6–0 ka BP were proposed for both units, respectively, based on 14C dating on sediment cores retrieved in similar settings in the NW Aegean Sea (Lykousis et al., 2005). Another timing for the last post-glacial transgression in the area has been proposed based on several 14C dates of sediment cores taken at different places in the Gulf of Corinth (Schwartz and Tziavos, 1979; Collier et al., 2000; Lemeille et al., 2004; Moretti et al., 2004; Van Welden, 2007; Campos et al., 2013a). Those dates converge toward a transgression of the two shallowest sills (Acheloos–Cape Pappas and Rion sills, Fig. 1B) around 11.5 ± 1 ka BP uncalibrated (Cotterill, 2006), which is coherent with the global sea level reconstruction from Siddall et al. (2003).

3. Data and methods

Seismic profiles and gravity cores were collected in the study area to investigate the possible influence of bottom currents on the Holocene sedimentation at different scales, from large sedimentary bodies to sediment samples. Published conductivity, temperature, depth data (CTD) and Google Earth satellite images of river sediment plumes were used to highlight indications about possible water circulations in the Gulf.

3.1. Seismic profiling

Six hundred kilometers of high-resolution single-channel reflection seismic profiles were acquired in 2011 and 2012 (Fig. 2). A multi-

electrode sparker was used as seismic source. It produces an acoustic signal with a mean frequency at 1.3 kHz, allowing to image up to 360 m of sediments with a vertical resolution of ca. 1 m. This seismic dataset was also used to build a bathymetric map of the study area.

We used the seismic-stratigraphic framework developed by Beckers et al. (2015) (Section 2.4.) to construct a detailed isopach map for the Holocene deposits in the study area. A morphosedimentary map of the Holocene deposits was also produced through the interpretation of the bathymetry, the seismic facies and the integration of previous works (Fig. 3B; Heezen et al., 1966; Lykousis, 1990; Piper et al., 1988, 1990; Lykousis et al., 2007b, 2009) and new coring data.

3.2. Gravity coring and sediment analysis

Twelve cores from 0.4 to 2.2 m long were retrieved in 2011 and 2014 with UWITEC® and BENTOS® gravity corers. The cores are located at various depths and various distances from the Rion straits, in order to investigate the sediment properties and the possible indications of bottom currents action in various settings (Fig. 2). Among the 12 cores, three are used to place constraints on the timing of the post-glacial sedimentary infill near the straits (NAF6, NAF7 and NAF10, Fig. 2). AMS radiocarbon dating was performed on two samples from NAF10 (bulk and shell) at the ARTEMIS facilities, France. Seven other cores retrieved in different sedimentary environments have also been analyzed: PSA01, NAF05, PSP05, PSP02, PSP03, TRZ03 and AEG02b (location in Fig. 2). X-ray photographs were taken from half core sections. Grain-size was measured by laser diffraction with a MALVERN™ Mastersizer 2000 device. Grain-size distribution parameters were obtained with the Gradistat software (Blott and Pye, 2001). Bulk mineralogy was measured on powders (<250 μm) by X-ray diffraction (XRD) on two other cores retrieved close to the northern coast (TRZ05, 65 cm long) and on the southern shelf (AEG01, 55 cm long) in order to highlight possible contrasts in mineral content between both sides of the Gulf (location in Fig. 2). Thirteen samples were measured in each core, each 5 cm downcore.

3.3. Anisotropy of magnetic susceptibility (AMS) and remanent magnetism

The anisotropy of magnetic susceptibility (AMS) was measured on 115 samples from 6 cores to detect a possible specific fabric interpreted in terms of bottom currents evidence (e.g. Shor et al., 1984). The paleodeclination of the remanent magnetism was measured on 4 of those 6 cores (PSA01, PSP05, PSP02 and TRZ03) in order to realign some AMS results into geographic coordinates. Magnetic susceptibility is a measure of the extent to which a material can be magnetized in relation to a given applied magnetic field. While its absolute value is a function of the content in magnetic grains, as well as their size, shape and nature, its anisotropy mainly provides information about the arrangements of the grains. AMS is a second-rank tensor, which is usually represented as an ellipsoid. AMS is specified by six parameters describing this ellipsoid, three relating to the magnitude of the principal susceptibility axes (K_{max}, K_{int}, K_{min}) and three relating to their directions, which are orthogonal. In sedimentology, AMS is assumed to reflect the average orientation of the magnetic grains that compose the sediment, with the maximum-susceptibility axis, K_{max}, and the minimum-susceptibility axis, K_{min}, representing the average orientation of the longest and shortest magnetic grain axes, respectively (Hamilton and Rees, 1970; Dall'olio et al., 2013). In marine settings, grain orientation is determined by the settling of the grain in the water column by gravity, the geomagnetic field, and currents. Grain orientation may also be modified during particle deposition on the seafloor, or after deposition by biological and physical processes (Ellwood and Ledbetter, 1977). Re-settling under specific conditions of re-suspended clay–silt fraction (<62 μm) may lead to a strong anisotropy especially with a high content of phyllosilicates (clay minerals) (Campos et al., 2013b). AMS has been widely used to determine the direction of bottom-currents (e.g. Rees, 1961; Ellwood, 1980; Flood et al., 1985; Parés et al., 2007; Singsoupho et al., 2015). K_{max} axes generally are oriented parallel to the current direction, but the grains may evolve into a flow-transverse orientation if the flow velocity is high enough to displace the grains on the seafloor after their initial deposition (Ledbetter and Ellwood, 1980; Taira, 1989; Tauxe, 1998; Baas et al., 2007).

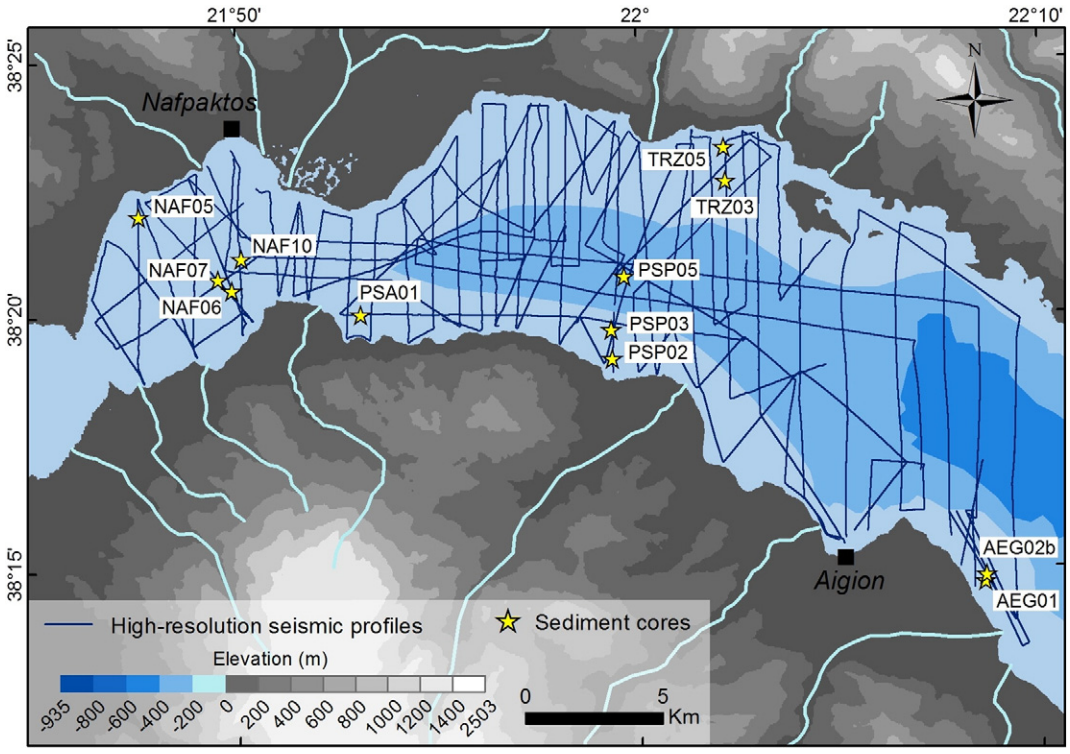

Fig. 2. Grid of high-resolution seismic profiles used in this study and location of the short gravity cores.

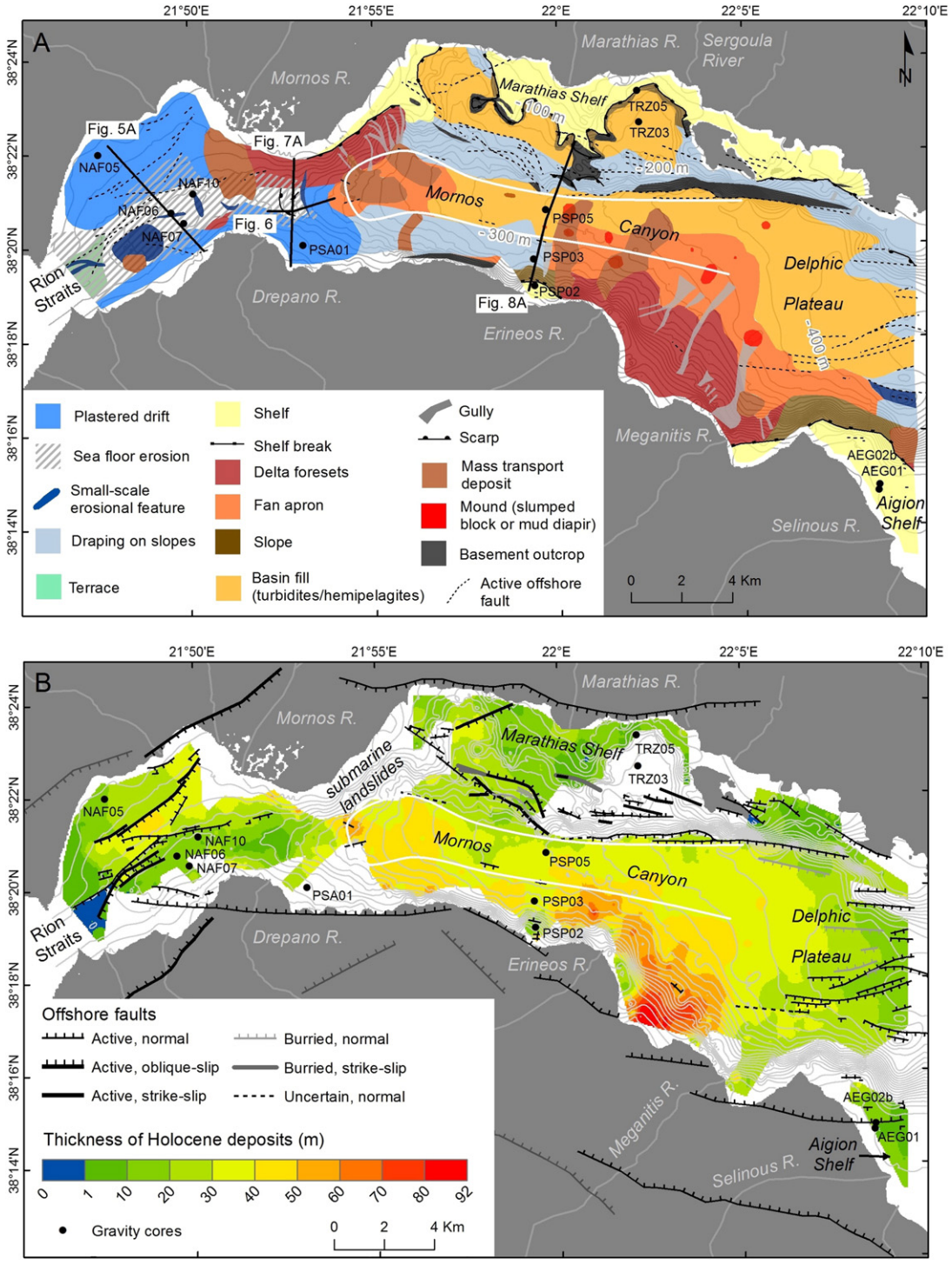

Fig. 3. A) Morphosedimentary map of Holocene deposits at the western tip of the Gulf of Corinth based on the interpretation of seismic profiles and short sediment cores (black dots). Boundaries between classes of deposits generally are progressive, i. e. between sediment drift deposits and draping on slopes, or between fans' apron and basin fill deposits due to lateral shifts during the Holocene. B) Thickness of Holocene deposits at the western tip of the Gulf of Corinth from the interpretation of Sparker seismic profiles, assuming an average acoustic wave velocity of 1600 m s^{-1} (stratigraphy from Beckers et al., 2015).

The six investigated cores were first sampled by 2 adjacent U-channels. One was used for paleomagnetic measurements, while the second was further sub-sampled for AMS analysis with $2 * 2 * 2$ cm plastic cubes. The AMS measurements were performed using an AGICO MFK1-FA Kappabridge (spinning specimen method). The natural remanent magnetization (NRM) was measured at the CEREGE paleomagnetic laboratory (Aix-Marseille University, France) in order to reorient the K_{max} axes of the AMS ellipsoid with regard to the magnetic north. Magnetization was measured on 0.6 to 1.0 m long U-channels using a superconducting quantum interference device (SQUID) pass-through cryogenic magnetometer (2G 760R), located in a shielded room. U-channel samples were subjected to stepwise alternating field (AF) demagnetization of the NRM using 4 to 7 steps. The characteristic remanent magnetization (ChRM) was extracted through a PCA analysis on demagnetization steps selected visually on Zijderveld diagrams in the PuffinPlot software (Lurcock and Wilson, 2012). The average

declination of the ChRM was calculated using Fisher statistics and used to reorient the AMS ellipsoid axes.

3.4. Oceanographic data

CTD profile data are available for the Gulf of Corinth through the World Ocean Database (http://www.nodc.noaa.gov/). The Ocean Data Viewer software was used to draw temperature, salinity and potential density anomaly sections (Schlitzer, 2015). These data make it possible to investigate possible relationships between water stratification and the sedimentary processes revealed by the seismic data. In the area of this study, thirty-four temperature and salinity profiles have been measured between 1909 and 2005 at different seasons. Only data measured in summer are sufficient to allow interpolating a profile along a section across the Gulf. This section crosses the Nafpaktos Bay in a NW–SE direction and is based on 8 CTD profiles. The lower data density in the rest of the study area did not permit to make N–S sections elsewhere.

The Google Earth satellite imagery database has been consulted in order to find possible images of river sediment plumes deflected by surface currents. Two examples of such a drift were found: the Mornos River sediment plume in March 2006 and the Fonissa River sediment plume in February 2014 (location of the river mouth in Fig. 1C).

4. Results

4.1. Seismic analyses

Seismic data allowed identifying different morpho-sedimentary environments. Fig. 3A shows the distribution of the main morpho-sedimentary units outcropping at the seafloor in the whole study area, while Fig. 4A is the same map zoomed in the area of the Nafpaktos Bay and the Mornos–Drepano sill. The morphology and the seismic characteristics of the morpho-sedimentary units will be described from west to east in this section, while our interpretations follow in Section 5.

4.1.1. Nafpaktos Bay and Mornos–Drepano sill

The general morphology of the Nafpaktos Bay is marked by a 2.5 km wide U-shaped valley striking NE–SW (Figs. 4A and 5A). The valley forms an 11 km long corridor, ranging in depth from ~40 m to ~115 m, i.e. the bottom of the Nafpaktos Bay, and extending from the Rion sill in the west to the Mornos–Drepano sill in the east (Fig. 4A). The seismic facies of sedimentary units that crop out in the axis of this valley consist of discontinuous, strong reflectors to the west, close to the Rion straits (e.g. Fig. 4B and C) and sub-parallel continuous reflectors to the east (Fig. 4D).

4.1.1.1. Erosive features. Terraces and smaller-scale erosional morphologies are observed in the axis of the U-shaped valley (dark blue features in Fig. 4A labeled f1 to f5). In the Rion sill area, the sea-floor morphology shows two sub-horizontal surfaces (terraces, Fig. 4B) separated by small mounds and by two elongated depressions. The two terraces are located at 62 to 71 m bsl. The two elongated depressions are 4 to 12 m deep and ~100 m wide and they merge toward east (f1, Fig. 4B). About 1 km to the northeast of the terraces, the seafloor is marked by a large circular depression named "f2" (Fig. 4A). The depression is 1.6 km wide and 35 m deep (Fig. 4C). This erosional feature is carved into a seismic unit made of high-amplitude chaotic reflections and is limited to the south by a MTD (Fig. 4C). In the eastern half of the Bay, the f3, f4 and f5 erosional features have similar characteristics (Fig. 4D and E). They are elongated depressions, 150–300 m wide, about 1 km long and 4–27 m deep. Depressions f3 and f5 strike E–W, while f4 strikes perpendicularly (Fig. 4A). These three erosional features are incised in a seismic unit essentially composed of parallel, continuous moderate amplitude reflectors (Fig. 4D and E). In the case of f4 and f5, higher-amplitude, sigmoidal reflections are also present on one side of the depression (Fig. 4E). The dense grid of seismic data acquired in this area shows that these three depressions are not connected to each other (Fig. 4A). Finally, other erosional features are observed east of the Nafpaktos Bay, just east of the Mornos–Drepano sill (Figs. 4A and 6). Here, the seafloor shows the following features: a curved N–S striking erosional scarp, a buried scour, and an active scour, labeled "f6" in Fig. 4A. Both scours strike parallel to the scarp and are consequently also parallel to the contour lines (Figs. 4A and 6). The scours are ~200 m wide, about 1.7 km long and 6–10 m deep. East of the scours, downslope, the seafloor is not eroded and sedimentary units composed of strong reflectors accumulate on top of the Holocene transgressive surface (Fig. 6).

4.1.1.2. Depositional features. Depositional reliefs, considered as drift deposits or contourite drifts, are present to the north and south of the U-shaped valley described above (in mid-blue in Figs. 3A and 4A). They form two elongated upward-convex reliefs striking parallel to the axis of the Gulf: the northern and the southern drifts. The northern drift is limited to the Nafpaktos Bay. It is 6 km long, 3 km wide and extends from the Rion straits to the Mornos River delta. The seismic units that compose the relief are up to 45 m thick. They onlap the Last Sea Level Rise unconformity already identified by Beckers et al. (2015) (Fig. 5A, LSLR: last sea level rise). The southern drift is longer than the northern one. It extends along 11 km from the Rion straits to the west to 3 km east of the Drepano delta to the east (Fig. 4A). In the Nafpaktos Bay, this depositional relief is relatively narrow (less than 1 km) and thin (less than 20 m of sediments above deltaic deposits, Fig. 4C). Eastward, east of the Mornos–Drepano sill, the southern drift is wider (up to 3 km) and also covers the axis of the Gulf in addition to its southern flank (Fig. 4A). This depositional relief is the thickest on the eastern flank of the Drepano River delta (at least 50 m of sediments above deltaic deposits, Fig. 7A).

In terms of seismic characteristics, both the northern and the southern drifts are composed of moderately strong, continuous parallel reflectors locally separated by internal unconformities (Fig. 5A). Reflections thin basinward or are truncated at the seafloor (e.g. Figs. 4C, 5A and 7A).

4.1.2. The area from the Mornos–Drepano sill to the Delphic Plateau

East of the Mornos–Drepano sill, the Gulf deepens and widens (Fig. 1D). Different sedimentary environments can be distinguished based on the seismic facies and based on the morphology of the deposits.

Basin fill deposits are observed in the Mornos Canyon, in the Delphic Plateau and in two sub-basins located north of the Mornos Canyon (Fig. 3A). The thickness of these deposits above the last sea level rise surface is 20–50 m in the Mornos Canyon and a few to 30 m in the Delphic Plateau (Fig. 3B). In the sub-basins north of the Mornos Canyon, the LSLR surface has not been identified everywhere. Where this surface has been defined, the thickness of basin fill deposits above the latter surface is between 20 and 40 m. The seismic facies of these deposits consists of sub-parallel high-amplitude reflections with variable frequencies (e.g. Fig. 8A). Lenses of incoherent reflections are also present (Fig. 8A).

Draping sediments are present on the slopes north of the Mornos Canyon and north of the Delphic Plateau, as well as in one region south of the Mornos Canyon, between the southern sediment drift to the west and the Erineos fan-delta to the east (Fig. 3A). On the northern slopes, sediment thickness above the LSLR surface is lower than 20 m while it reaches 50 m on the slopes south of the Mornos Canyon. The seismic characteristics of these draping units are a lower amplitude and a better continuity of the reflections in comparison to Basin fill deposits, in addition to the draped pattern.

Other sedimentary environments are related to the existence of Gilbert-type fan-deltas, already described in details by Piper et al. (1990) and Lykousis et al. (2009). These environments are described here as shelves, delta foresets and fan aprons (Fig. 3A). Around the Mornos, the Erineos and the Meganitis fan-deltas, the shelf is almost

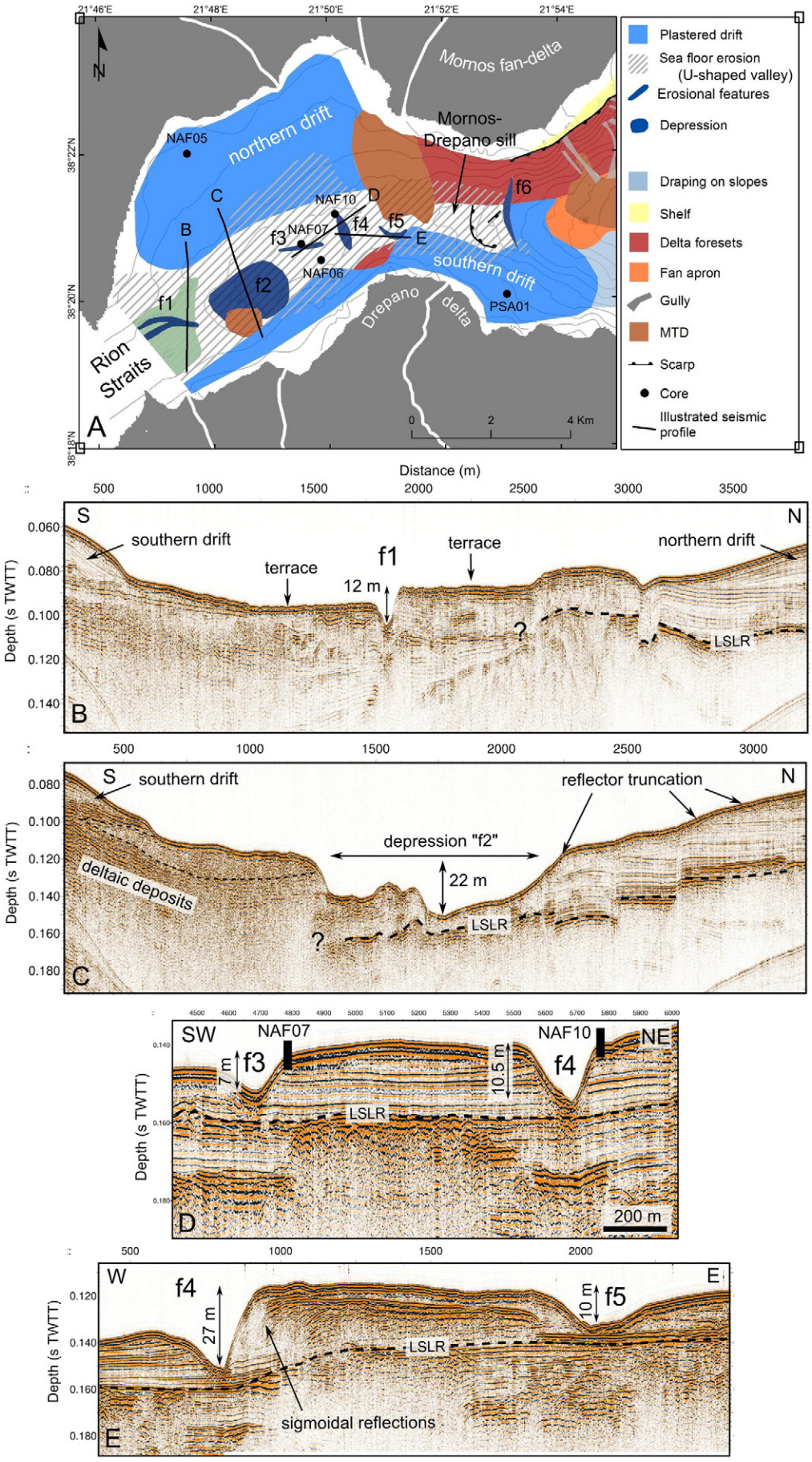
21°46'E
21°48'E
21°50'E
21°52'E
21°54'E
38°22'N
38°20'N
38°18'N
N
Mornos fan-delta
northern drift
Mornos-
Drepano sill
NAF05
NAF10
NAF07
NAF06
PSA01
f1
f2
f3
f4
f5
f6
B
C
D
E
southern drift
Drepano
delta
Rion
Straits
A
0
2
4 Km
Plastered drift
Sea floor erosion
(U-shaped valley)
Erosional features
Depression
Draping on slopes
Shelf
Delta foresets
Fan apron
Gully
MTD
Scarp
Core
Illustrated seismic
profile
Distance (m)
500
1000
1500
2000
2500
3000
3500
S
N
southern drift
terrace
f1
12 m
terrace
northern drift
?
LSLR
Depth (s TWTT)
0.060
0.080
0.100
0.120
0.140
B
4500
4600
4700
4800
4900
5000
5100
5200
5300
5400
5500
5600
5700
5800
5900
6000
S
southern drift
reflector truncation
N
depression "f2"
22 m
deltaic deposits
?
LSLR
0.080
0.100
0.120
0.140
0.160
0.180
C
SW
NAF07
NAF10
NE
7 m
f3
10.5 m
f4
LSLR
200 m
D
500
1000
1500
2000
W
f4
27 m
10 m
f5
E
LSLR
sigmoidal reflections
0.120
0.140
0.160
0.180
E

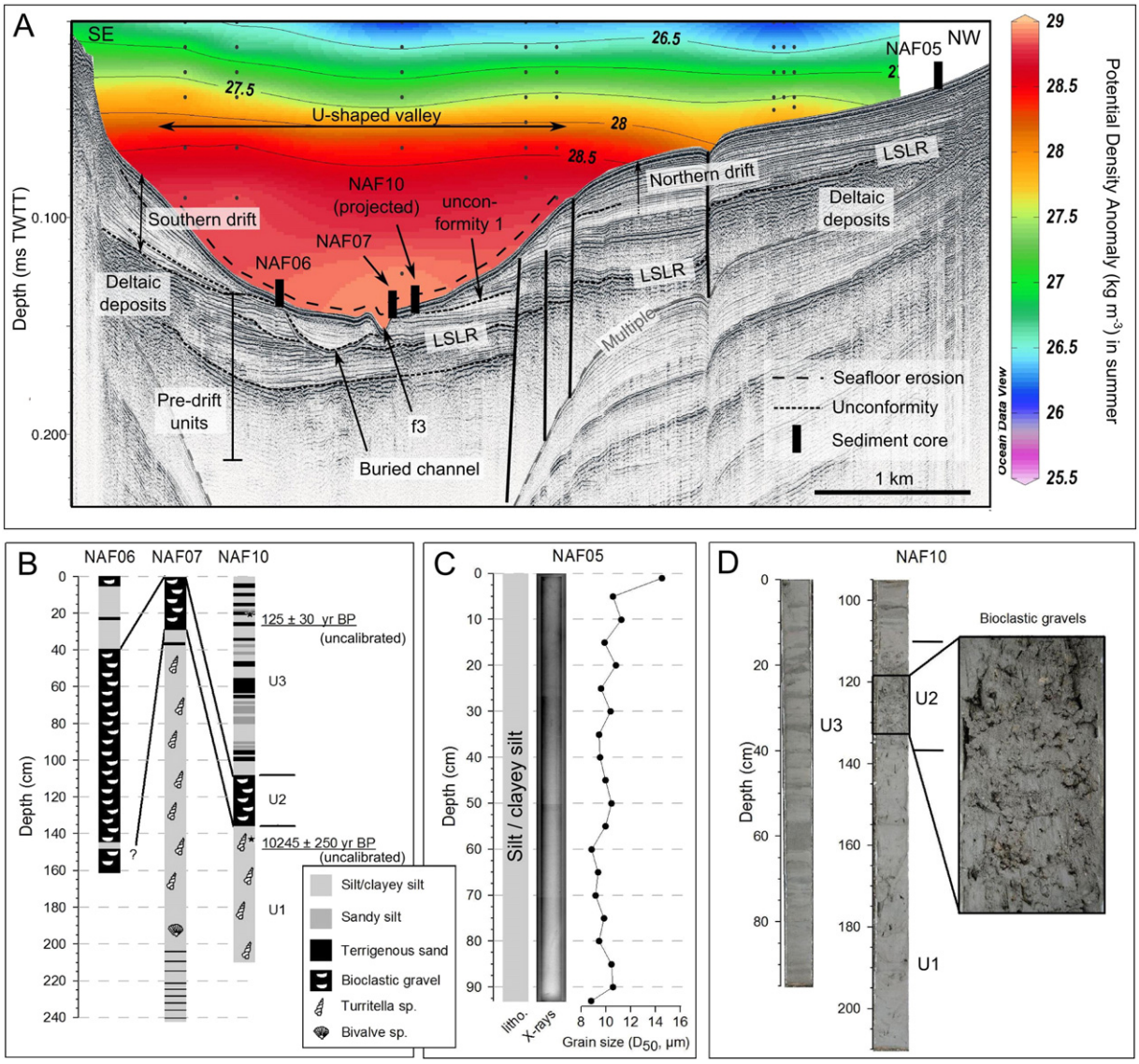

Fig. 5. Sparker seismic profile and sediment cores from the Nafpaktos Bay. A) Sparker seismic profile showing depositional reliefs interpreted as sediment drifts in the Nafpaktos Bay. LSLR: last sea level rise. Colors represent the potential density anomaly in summer inferred from 6 temperature and salinity profiles (black dots) from the World Ocean Database (http://www.nodc.noaa.gov/). Location of the profile in Fig. 3A. B) Logs and radiocarbon ages constrains of the three gravity cores retrieved in the center of the Nafpaktos Bay (for location see Fig. 4A). C) Lithology, X-ray picture and median grain-size of the core NAF05 retrieved in the northern sediment drift. D) Picture of the core NAF10 highlighting the sedimentary unit U2.

absent (Fig. 3A). Only some narrow shelf remnants (<1 km wide) exist on the side of these deltas, e.g. west of the Erineos fan and in the bay between the Meganitis and the Selinous fan-deltas (Fig. 3A). The shelf is wider around the Selinous and the Marathias fan-deltas, reaching 2 km wide.

The slopes that link the shelf edge to the Mornos Canyon or the Delphic Plateau generally consist of two morphosedimentary units that differ by the slope angle: relatively steep delta foresets and less steep fan aprons (Fig. 3A). In the Mornos fan-delta, delta foresets show different morphologies between the south-western and the south-eastern slopes. To the south-west, the foresets extent from the coast to about 100 m bsl and their slope angle is about 2.5°. Most of the foresets in this area are affected by a rotational slump evidenced by the presence of curved growth faults (see seismic profiles in Lykousis et al., 2009). To the south-east, the foresets extent deeper, reaching the Mornos Canyon at 170–200 m bsl. Their slope is steeper, reaching about 9°. The morphology of this flank of the Mornos delta is more irregular than the south-eastern flank. Foresets are affected by landslide head scars as well as numerous gullies (Fig. 3A). The seismic facies of the Mornos delta foresets is highly variable and encompass subparralel to chaotic reflections with variable amplitudes and frequencies. Along the opposite margin, in the Erineos fan-delta, the delta foresets extent from the coast to a depth of 310–340 m bsl and their slope angle ranges between 15 and 30°. Foresets are cut by gullies, mainly on the eastern flank of the delta, that merges with the Meganitis River prodelta (Piper et al., 1990). On the northern flank, foresets are disrupted by submarine landslide scars (Fig. 3A). Two MTDs related to these landslide scars outcrop at the seafloor downslope, in the Mornos

Fig. 4. Map view (A) and seismic profiles (B, C, D, E) illustrating the erosional features identified in the Nafpaktos Bay. LSLR = last sea level rise. MTD = mass transport deposit.

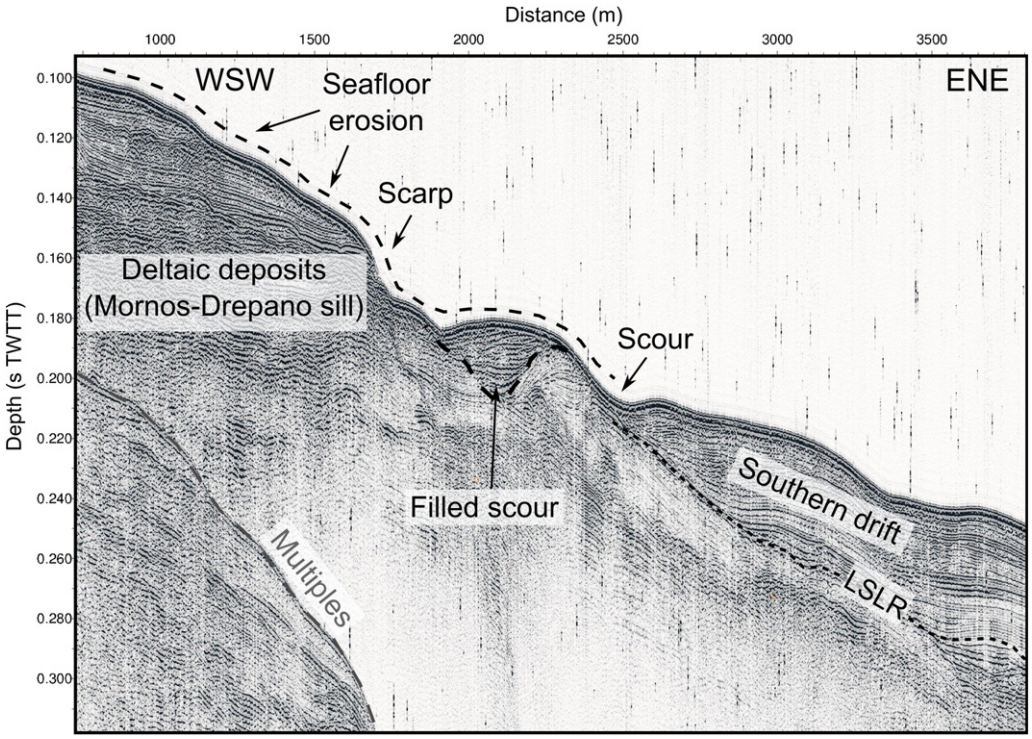

Fig. 6. Sparker seismic profile showing bedforms and a depositional relief interpreted as resulting from the action of bottom-currents on the eastern slope of the Mornos–Drepano sill. LSLR: last sea level rise. Location of the profile in Fig. 3A.

Canyon (Fig. 3A). Sediment thickness above the LSLR surface is particularly huge in the foresets located between the Erineos River mouth and the Meganitis River mouth, reaching locally 90 m (Fig. 3B). Foresets of both fan-deltas are imaged as variable amplitude, continuous parallel reflections (not illustrated here, see Piper et al., 1990 and Lykousis et al., 2009).

Fan aprons form a 2 to 3.5 km wide band south of the Delphic Plateau and south and west of the Mornos Canyon. These deposits are located between delta foresets, upslope, and basin fill deposits, downslope. They are characterized by a seafloor slope angle of 1.0–1.8° and a seismic facies that varies laterally between lenses of low-amplitude chaotic reflections, lenses of high-amplitude hummocky reflections, and wider units of subparallel continuous reflections.

Seismic profiles also reveal eleven mounded structures essentially located in the Erineos delta fan apron areas (Fig. 9B and C and map view in Fig. 3A). The accurate geometry of these reliefs is not constraint by this study, but seismic data suggest that they are about 100 to 750 m in diameter and 4 to 20 m high. Fig. 9B and C shows seismic profiles imaging the center of two of these mounded features. In both cases, the top of the mound is imaged as hyperboles. Seismic facies however differ between the two mounds. In Fig. 9B, the mounded feature is composed of high-amplitude incoherent reflections, similar to the seismic facies of a MTD outcropping at the seafloor at the same location, around the mound. In Fig. 9C, a similar seismic facies is present at depth, but the sediments just below the surface of the mound are imaged as parallel hyperboles, suggesting the existence of stratification.

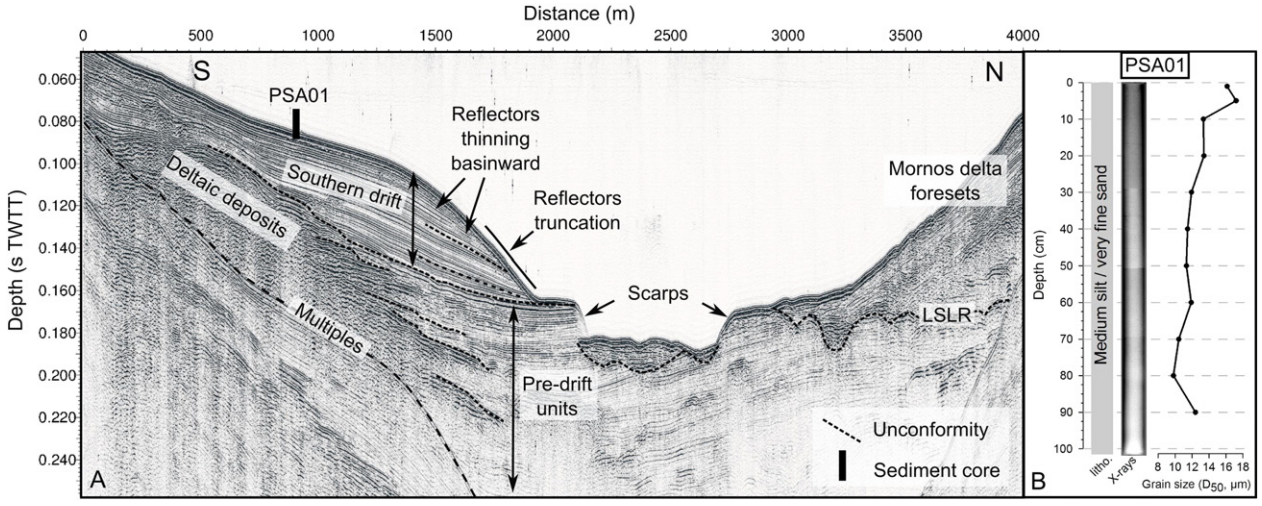

Fig. 7. A) Sparker seismic profile showing a depositional relief interpreted as sediment drift between the Drepano (to the south) and the Mornos (to the north) deltas. LSLR: last sea level rise. Location of the profile in Fig. 3A. B) Lithology, X-ray picture and median grain size for the core PSA01.

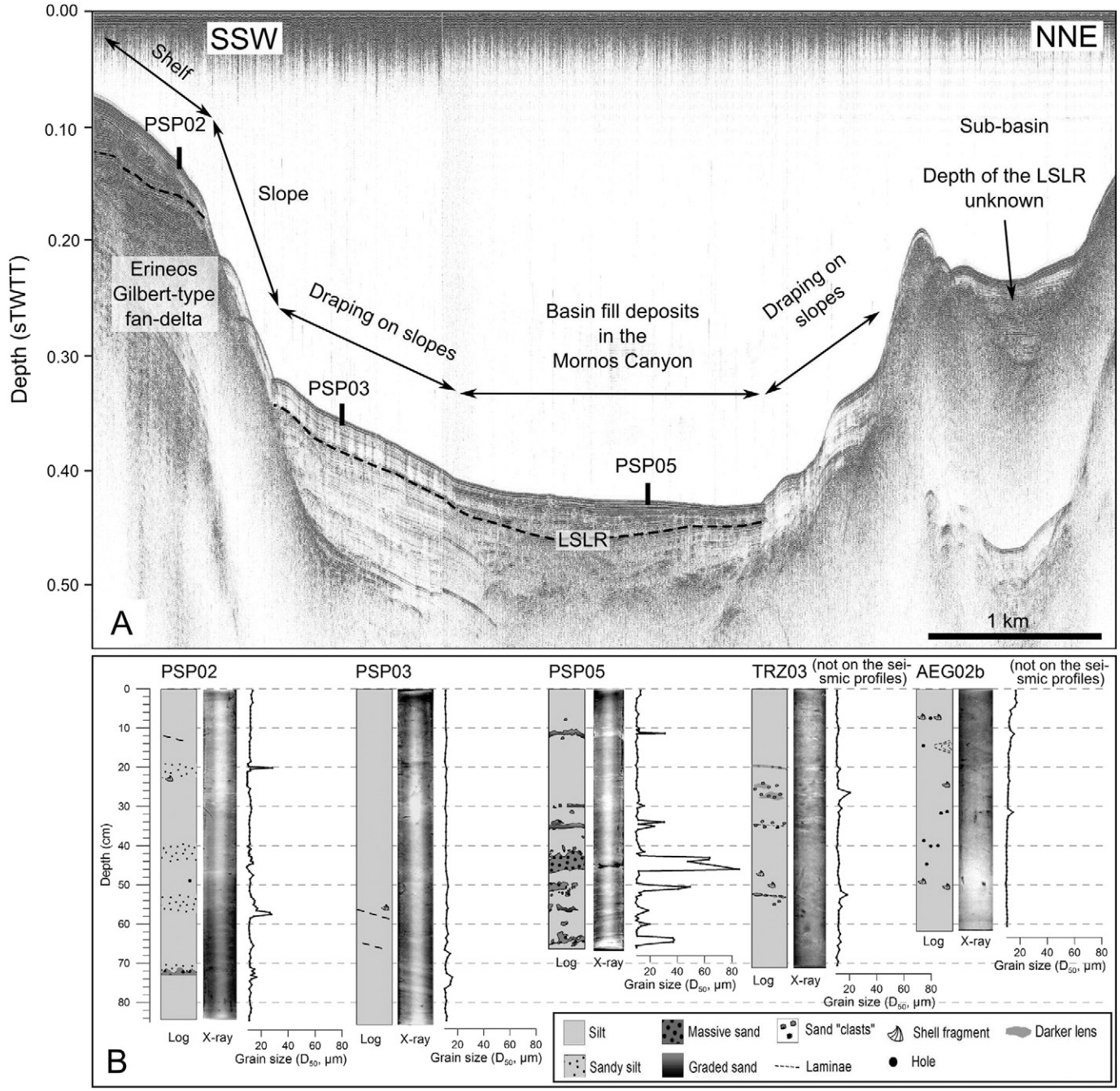

Fig. 8. A) Sparker seismic profiles illustrating the Mornos Canyon. LSLR = last sea level rise; MTD = mass transport deposit. Location in Fig. 3A. B) Lithology, X-ray picture and median grain size for five short cores retrieved in the study area (location in Figs. 2 and 3).

4.2. Sedimentary units in cores

In the central part of Nafpaktos Bay, three cores (NAF06, NAF07 and NAF10) have been retrieved, at 100–110 m bsl, where seismic data indicate seafloor erosion (Figs. 3A and 5A). The cores are located 0.7 to 1.7 km apart from each other and are 1.6 m, 2.4 m and 2.1 m long, respectively. They have been correlated with each other based on the visual description of their sedimentary facies (Fig. 5B). They show the following succession of sedimentary units from bottom to top (Fig. 5B). A first unit (U1) is composed of dark gray clayey silt. Thin layers of normally graded dark sands are present at the base of the unit, while the upper part consists of homogeneous clayey silt with numerous intact specimens of *Turritella* sp., which seem to be in undisturbed position. At the top of the unit, one *Turritella* sp. has been radiocarbon dated at 10,250 yr ± 250 BP (uncalibrated and uncorrected for reservoir effects). The second unit (U2) is composed of poorly sorted bioclasted gravels and shows a variable thickness, from 0.2 to at least 1.2 m (Fig. 5B and C). The third unit (U3) comprises a succession of massive and normally graded sandy layers, intercalated with gray mud. Dating on organic matter fragments retrieved from a sandy layer at 21 cm gives an uncalibrated age of 150 yr ± 30 BP.

The northern and southern contourite drifts of the Nafpaktos Bay have been respectively sampled by the cores NAF05 (93 cm long) and PSA01 (100 cm long) (location in Fig. 4A). Both cores show similar sedimentary characteristics in terms of grain size and structures. The cores are homogenous both with direct eye-observation and under X-rays.

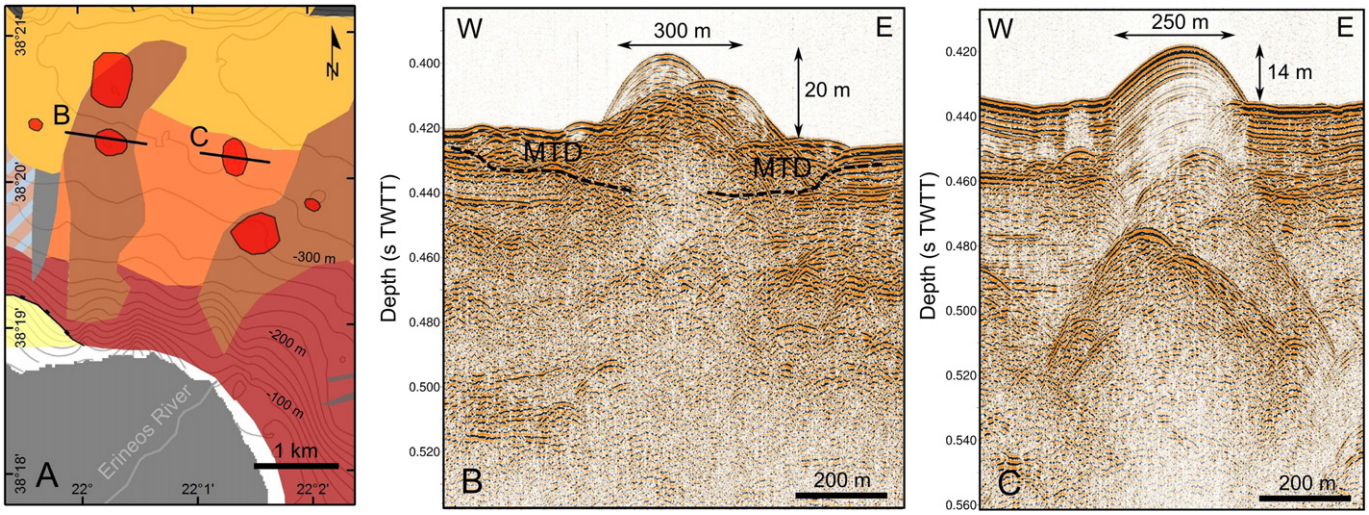

Fig. 9. Map view (A) and Sparker seismic profiles (B and C) showing two mounds in the prodelta of the Erineos River. See the legend of Fig. 3A for the color code of the map.

They are composed of light brown mud with a median grain size (D_{50}) between 8 and 18 μm (Figs. 5C and 7B).

Eastward, the cores PSP02, PSP03 and PSP05 sample the small shelf west of the Erineos fan-delta, the sediments draping the southern flank of the Mornos Canyon, and the basin fill deposits in the Mornos Canyon itself, respectively (Figs. 3A, 8). PSP02 (85 cm long) shows an alternation of light brown mud and slightly coarser-grained layers that are not particularly distinguishable on X-ray pictures (Fig. 8B). Sediment sampled in the core PSP03 (86 cm long) is homogenous to the naked eye, except a few thin darker laminae (Fig. 8B). Grain-size indicates silty sediments and confirms the facies homogeneity. X-rays reveal changes in density at the base of the core giving evidence for sediment stratification (Fig. 8B). PSP05 was retrieved in the Mornos Canyon, close to an outcropping MTD resulting from a sediment failure on the Erineos delta slopes (see the map view in Fig. 3A). The core contains an alternation of seven dark gray, 1 to 4 cm thick massive or

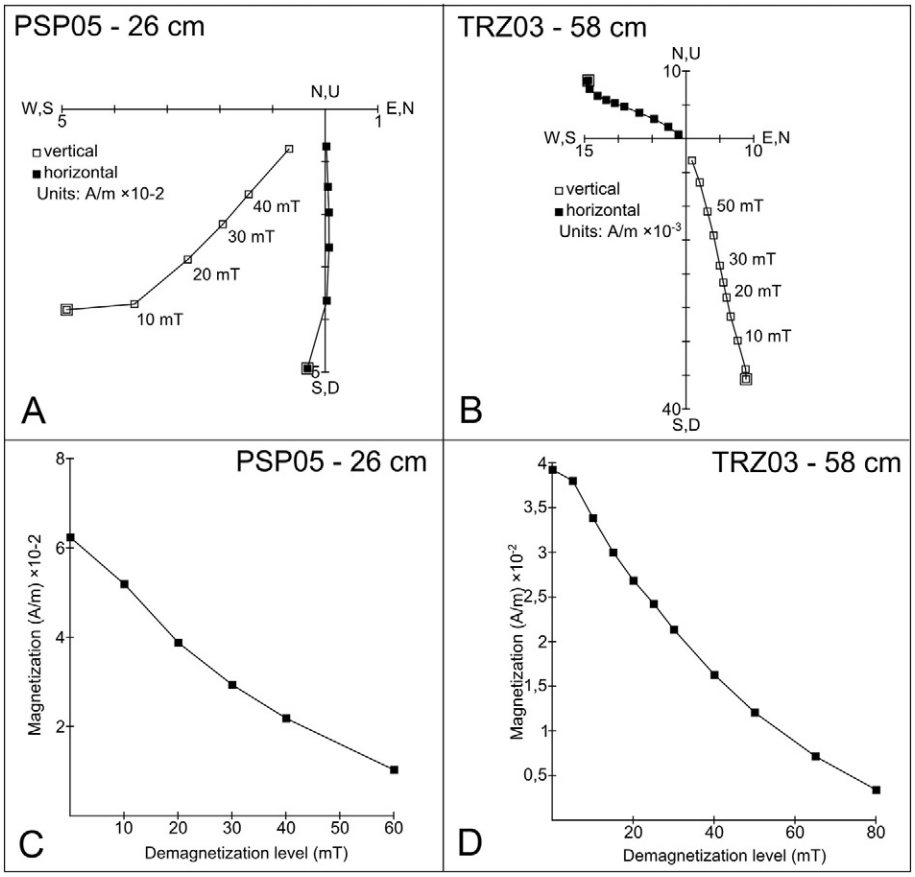

Fig. 10. Demagnetization plots of the natural remanent magnetization for two representative sediment samples in PSP05 and TRZ03. A) and B): Zijderveld diagrams showing the magnetization vectors at each demagnetization step projected on two orthogonal plans. Black squares correspond to the vertical plan while white squares correspond to the horizontal plan. C) and D): classical demagnetization plots.

normally graded sandy layers, and brown mud intervals (Fig. 8B). Some sandy layers are visible on the X-ray picture, either as high-density layer, in white, or in one case as a very low density layer, in black (at 44 cm, Fig. 8B).

Farther north, along the northern margin, the core TRZ03 (69 cm long) has been retrieved in the center of a sub-basin, west of the Trizonia Island (Fig. 3A). The core contains gray-brown mud with some 1–3 mm thick, highly bioturbated sandy layers, difficult to identify by the naked eye but imaged under X-rays, particularly between 18 and 38 cm (Fig. 8B).

The last core, AEG02b (61 cm long), has been taken on the shelf off the Selinous River mouth (Aigion Shelf, Fig. 3A). This shelf is characterized by pockmarks and mounds linked to the Aigion Fault (Cotterill, 2006). The core contains visually homogenous light brown mud (Fig. 8B). X-rays reveal some bioturbation holes as well as slump-like structures between 12 and 16 cm (Fig. 8B).

4.3. Mineralogy

Average XRD mineral compositions of TRZ05 and AEG01 are similar. Total clay minerals (mainly kaolinite and illite) represent the largest class in each core, with 35 and 32% in TRZ05 and AEG01, respectively. In TRZ05, the main other minerals are muscovite (31%), quartz (12%), calcite (8%), and plagioclase (7%). Those three minerals are also the most abundant in AEG01 after clay minerals, with light differences in concentrations. The other minerals identified in the two cores are K-feldspars and dolomite.

4.4. Remanent magnetization

Demagnetization paths for two samples (cores PSP05 and TRZ03) are illustrated in Fig. 10. The NRM shows two components. The component defined as the ChRM has been reached after the first steps of demagnetization, at 10 mT. The ChRM shows a linear trend toward the origin on the orthogonal plots. The median destructive field (MDF) of the NRM provides information on the mean coercivity state of the sample, which is a reflection of its grain size and mineralogy (Stoner and St-Onge, 2007). MDF varies between 20 and 38 mT along every core (PSA01, PSP02, PSP05 and TRZ03, Fig. 11).

Average orientations of the ChRM deduced from Fisher statistics are summarized in Table 1. In TRZ03, PSP02 and PSA01, the declination of the ChRM varies along core over a range of ~30°. Concerning the inclination of the ChRM, The mean inclination of the ChRM in the cores varies between 33 ± 1.1° (PSP05) and 65 ± 2.2° (PSA01) (Table 1).

4.5. AMS

Table 2 presents the AMS parameters averaged for each core. All samples show a significant tri-axial anisotropy at the 5% confidence level according to the F, F12, and F23 tests (Hext, 1963). Mean values of anisotropy (P), lineation (L) and foliation (F) are the largest in the southern drift (core PSA01) and the lowest in the Aigion Shelf (core AEG02b). The shape of the ellipsoid of anisotropy is mainly oblate for specimens in TRZ03, PSA01, PSP02 and PSP03 (T > 0), while the values of T are more scattered in PSP05 and AEG02b, with positive and negative values. The orientation of the K_{max}, K_{int} and K_{min} axes gives more insights in the possible depositional processes acting at each site. Those axes are plotted in Fig. 12 in a lower-hemisphere projection, in the core coordinate system (i.e. without correction). Red symbols represent specimens sampled in a coarser-grained layer while the other colors correspond to fine-grained sediments. Their distribution in the six diagrams shown in Fig. 12 suggests that the magnetic fabric is similar between fine-grained intervals, i.e. the background sedimentation, and coarse-grained layers. AEG02b is the shallowest coring site, at −40 m. Specimen K_{min} axes, that theoretically are oriented near the vertical in deep-water hemipelagites not influenced by bottom currents,

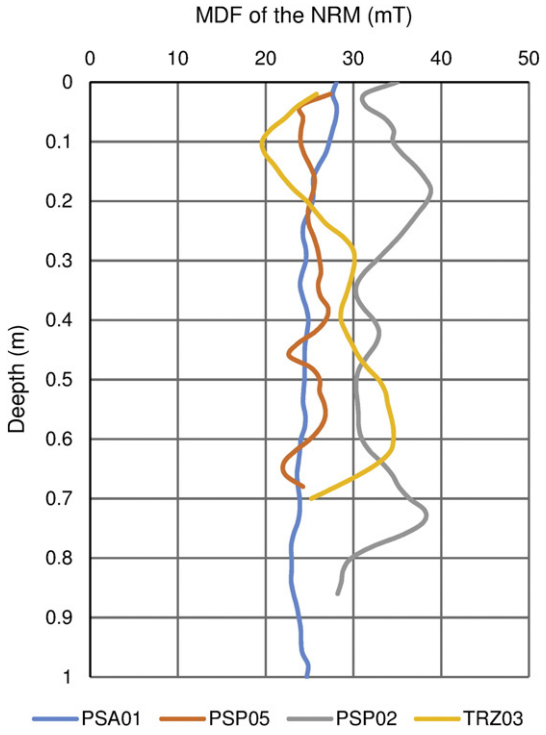

Fig. 11. Median destructive field of the natural remanent magnetization of the 4 cores whose characteristic remanent magnetization has been extracted. See Figs. 2 and 3 for core location.

are scattered with an average inclination of 79° (90° means a vertical K_{min}). This scattering may be partly explained by the low value of anisotropy (around 1%). Most of the K_{max} axes are subhorizontal and their azimuths, even if scattered, show coherent values along core. PSP02 is located at −100 m, on a small shelf on the southern gulf margin that is sloping to the north at an angle between 5 and 10°. K_{min} axes are tilted, with an average inclination of 65°. K_{max} axes are subhorizontal, slightly tilted. K_{max} azimuths are very coherent along core. In PSP05, in the Mornos Canyon, K_{min} axes are subvertical. K_{max} axes also have the same azimuths along core. In the Trizonia sub-basin, core TRZ03, the pattern of anisotropy is intermediate between those of PSP05 and AEG02b. The K_{min} axes are subvertical, similarly to PSP05, and the K_{max} axes are subhorizontal but more scattered in azimuth, similarly to AEG02b. In the sediments draping the slopes, core PSP03, K_{min} axes are slightly tilted (average inclination = 78°), and K_{max} axes show the same direction along the core, similarly to the pattern of K_{max} in PSP05. Finally, PSA01, in the southern sediment drift shows the same AMS pattern as PSP05: K_{min} axes are near vertical and the declination of K_{max} does not vary with depth.

Based on the average declination of the ChRM, K_{max} axes of four cores have been oriented with regard to the magnetic north (Fig. 13). K_{max} axes show variable orientations relatively to the slope of the seafloor. They are parallel to the slope direction in the Mornos Canyon (PSP05) and roughly perpendicular (i.e. parallel to the isobaths) in the Trizonia sub-basin (TRZ03). In the southern sediment drift (PSA01)

Table 1
Average orientation of the characteristic remanent magnetization (ChRM). N: number of samples; k: precision parameter; alpha95: 95% confidence limit.

Core	Dec ChRM (°)	Inc ChRM (°)	N	k	alpha95
TRZ03	285	50	30	176	2
PSA01	210	65	45	106	2.1
PSP02	119	45	38	41	3.7
PSP05	177	33	29	606	1.1

Table 2
Averaged results (mean ± standard deviation) of the anisotropy of magnetic susceptibility measurements. See the text for the description of the parameters.

Core	N	Bulk MS (10^{-6} SI)	L	F	P	T	Dec K_{max} (°)	Conf angle (°)	Inc K_{min} (°)	Conf angle (°)
AEG02b	25	264 ± 32	1.005 ± 0.002	1.006 ± 0.003	1.011 ± 0.004	0.052 ± 0.418	276	20.6	79	15.7
TRZ03	23	207 ± 29	1.006 ± 0.002	1.011 ± 0.004	1.017 ± 0.004	0.286 ± 0.281	317	24.3	85	7.9
PSP05	34	250 ± 40	1.013 ± 0.003	1.012 ± 0.007	1.025 ± 0.008	−0.102 ± 0.324	82	7.9	81	4.3
PSP03	12	296 ± 25	1.010 ± 0.003	1.018 ± 0.008	1.028 ± 0.010	0.257 ± 0.253	89	4.6	78	3
PSA01	11	364 ± 49	1.016 ± 0.003	1.026 ± 0.004	1.043 ± 0.007	0.237 ± 0.080	271	4.8	89	2.3
PSP02	47	214 ± 27	1.009 ± 0.004	1.014 ± 1.005	1.023 ± 0.005	0.232 ± 0.360	91	9.5	65	5.9

and in the Erineos Shelf (PSP02), K_{max} orientation seems to be oblique with regard to the slope direction.

4.6. Oceanographic data

The potential summer water density anomaly in the Nafpaktos Bay increases from the sea surface to about 80 ms TWTT (−60 m) and stabilizes below (Fig. 5A). This pattern essentially results from an exponential decrease in temperature with depth (Fig. 14A). Salinity varies very few with depth, between 38.2 and 38.6 psu. One maximum is observed at a depth of about 50 m (Fig. 14B).

Both the Mornos River sediment plume in March 2006 (Fig. 15A) and the Fonissa River sediment plume in February 2014 (Fig. 15B) are deviated toward the east (location of the rivers in Fig. 1C). This indicates the existence of significant surface currents flowing eastward during these two periods.

5. Interpretations

5.1. Bottom-current related morphologies and shallow water contourite drifts

5.1.1. Erosional features

Several observations support that the wide U-shaped valley located in the Nafpaktos Bay and on the Mornos–Drepano sill is an area of seafloor erosion, or locally sediment non-deposition. The most obvious evidence is the reflectors truncation observed on the flanks of the valley in several seismic profiles (e.g. Figs. 4C and 5A). Another argument in favor of a significant erosion of Holocene sediments is the low thickness of Holocene deposits revealed by the isopach map in the center of the Nafpaktos Bay (10–15 m of Holocene sediment) as well as in the Mornos–Drepano sill (5–10 m of Holocene sediment) (Fig. 3B). Besides, the analysis of the cores NAF06, NAF07 and NAF10 confirms the very restricted accumulation of sediments (locally less than 1 m) in the center of the Nafpaktos Bay since about 10 ka BP (uncalibrated). In the Rion straits area, most seismic units outcropping at the seafloor are interpreted as relatively coarse-grained pre-Holocene sediment (blue area in Fig. 3B). The area affected by seafloor erosion corresponds to the area where strong currents have been reported (Fig. 1C). It is consequently proposed that bottom currents are a major control on the seafloor morphology in the Nafpaktos Bay and Mornos–Drepano sill areas.

The smaller erosional features f3, f4 and f5 are interpreted as furrows (Fig. 4A). The arguments for this interpretation, rather than an interpretation in favor of channels, are their small depth, the absence of levees in many cases and the fact that they are disconnected from each other. The presence of furrows indicates the existence of bottom currents, and particularly the role of secondary helical circulation in the boundary layer of the bottom currents (Flood, 1983). The depression f2 may result from another type of secondary circulation, or from the action of the bottom-currents itself, considering the wide spatial extent of the depression (Fig. 4A and C). The erosional feature f1 is locally carved in a pre-Holocene substratum (Fig. 4B). It has been interpreted by Perissoratis et al. (2000) as a fluvial outlet channel of the Lake Corinth, which occupied the Gulf during Quaternary lowstands. Finally, it is proposed that the curved scarp and the scours located just east of the Mornos–Drepano sill (Fig. 6) result from turbulence that develops at the exit of the sill due to the sudden increase in seafloor slope angle. The scarp may also initially result from a slope failure (see a more detailed discussion about these features in Section 5).

5.1.2. Depositional features

Based on their convex morphology, on the seismic facies and on their location along an area influenced by bottom currents, it is proposed that the two depositional reliefs that occur in the north and south of the Nafpaktos Bay, around the Drepano River delta and east of the Mornos–Drepano sill, are shallow-water contourite drifts (Fig. 4A). Cores NAF05 and PSA01 give clues on the nature of these sediment bodies. Both cores show that the seismic facies of the two sediment drifts represents, at least for the upper parts of the deposits, homogenous, structureless muddy sediments (Figs. 5C and 7B). The spatial configuration of the two sediment drifts indicates that the sediments essentially accumulate in the north of the Nafpaktos Bay (northern sediment drift, Fig. 4A) and east of the Drepano delta (southern sediment drift, Fig. 4A), which probably creates a protected area where sediment deposition is possible.

In the Mornos–Drepano sill area, a strong N–S asymmetry in sedimentary processes exists (Fig. 7A). To the north, the slope is composed of unstable coarse-grained sediments forming the Mornos delta foreset beds, while to the south, the thick southern sediment drift develops on top of deltaic deposits. East of the Mornos–Drepano sill, Holocene deposits are also interpreted as sediment drifts because of the wavy pattern of the seafloor and the underlying reflections, adjacent to two elongated erosional features (Fig. 6).

No other depositional relief or erosional bedform possibly resulting from the action of bottom currents has been identified east of the southern sediment drift (Fig. 4A).

5.1.3. Possible direction of bottom currents that generate erosive and depositional features

The spatial distribution of sediment drifts and erosional features allow to estimate the average orientation of bottom currents in the Gulf of Corinth during the Holocene. In the Rion sill, the absence of sediment drift suggests that bottom currents flow across the entire strait. In the Nafpaktos Bay, the asymmetry between the well-developed northern drift and the narrower southern drift shows that bottom currents flow closer to the south-eastern coast, following the deepest part of the Nafpaktos Bay. The direction of the flow(s) in this area is consequently NE–SW and/or SW–NE. Eastward, bottom-currents cross the Mornos–Drepano sill and are responsible for the development of sediment drifts on the southern flank of the Gulf as well as in the Gulf axis, on the eastern slope of the sill.

5.1.4. Sedimentary units at the bottom of the Nafpaktos Bay

The three cores retrieved in the center of the Nafpaktos Bay (NAF06, NAF07 and NAF10, Fig. 5) give clues to interpret the different seismic facies in terms of sediment characteristics, sedimentary processes, and ages of seismic units. Three sedimentary units (U1, U2, U3) have been defined and are interpreted as follow. In Unit 3, which has only been found in NAF10, the alternation between fine-grained intervals and sandy layers (Fig. 5B and D) could be interpreted either as fine-grained hemipelagites interbedded with thin-bedded turbidites/debrites or as contourites. Indeed, the seafloor relief and the seismic

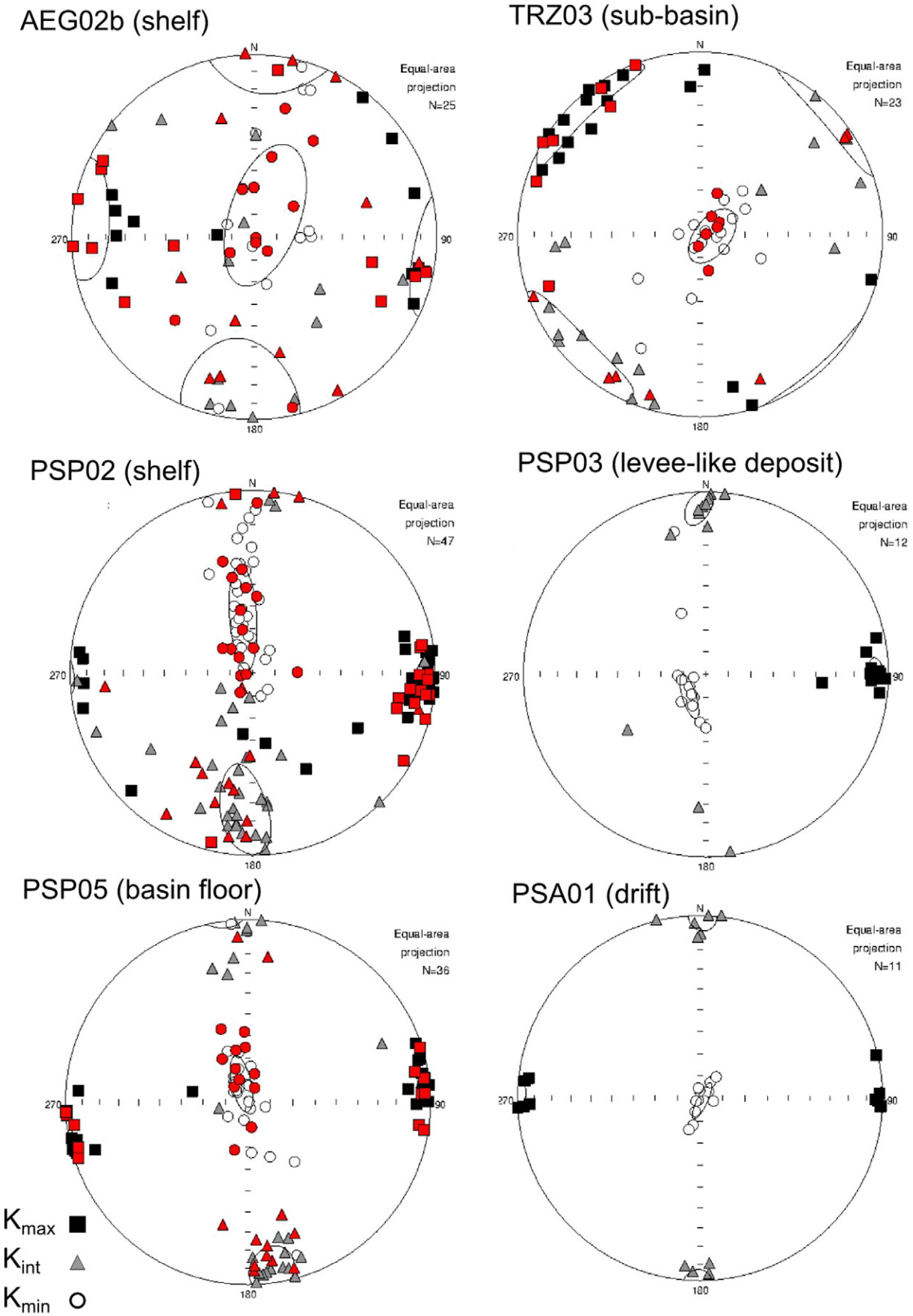

Fig. 12. Unoriented anisotropy of magnetic susceptibility of recent sediments in 6 cores from the western Gulf of Corinth. The axes of anisotropy are plotted in a lower hemisphere stereographic projection. Red dots correspond to cubes sampled in coarser-grained layers (sand) interpreted as event deposits while the other colors (white, gray, black) correspond to cubes sampled in fine-grained intervals. See Figs. 2 and 3 for core location.

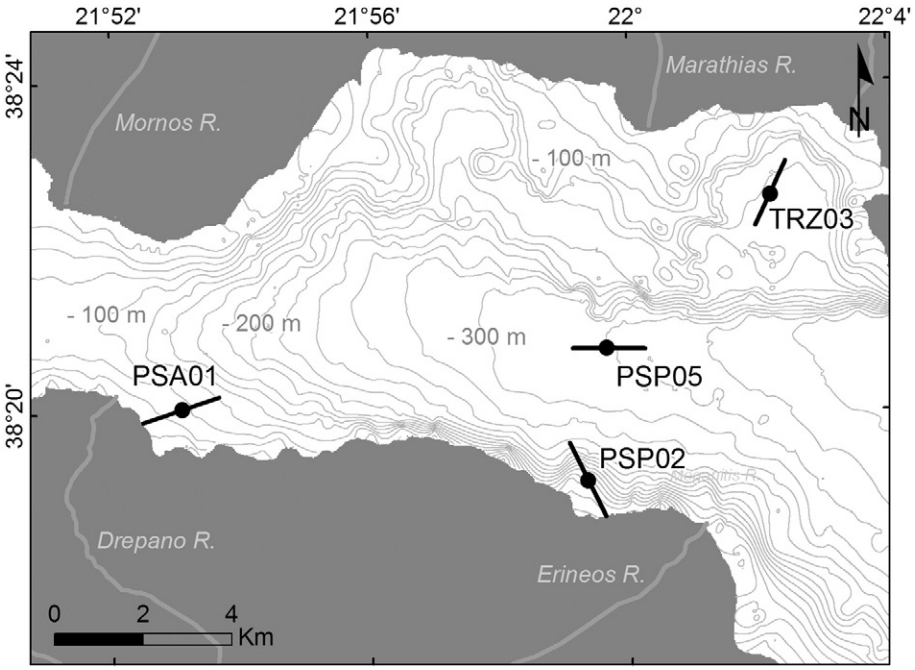

Fig. 13. Average orientation of maximum-susceptibility axes (K_{max}) for 4 short gravity cores in the western tip of the Gulf of Corinth. The cores are 0.65 m to 1.0 m long and the anisotropy of magnetic susceptibility has been measured on 11 to 47 samples from each core. In each core, K_{max} axes follow a unique direction (see Fig. 12) that has been re-oriented with respect to the magnetic north based on the declination of the characteristic remanent magnetization. The bathymetry has been interpolated from the grid of seismic data (see the grid in Fig. 2).

facies characteristics in the center of the Nafpaktos Bay are compatible with the existence of both turbidity currents coming from the Mornos prodelta slopes and with contourites deposited by bottom currents in the axes of the Bay. Moreover, distinguishing contourite facies from turbidite facies in sediment cores still suffer from a lack of unambiguous and commonly accepted diagnostic criteria (e.g. Rebesco et al., 2014).

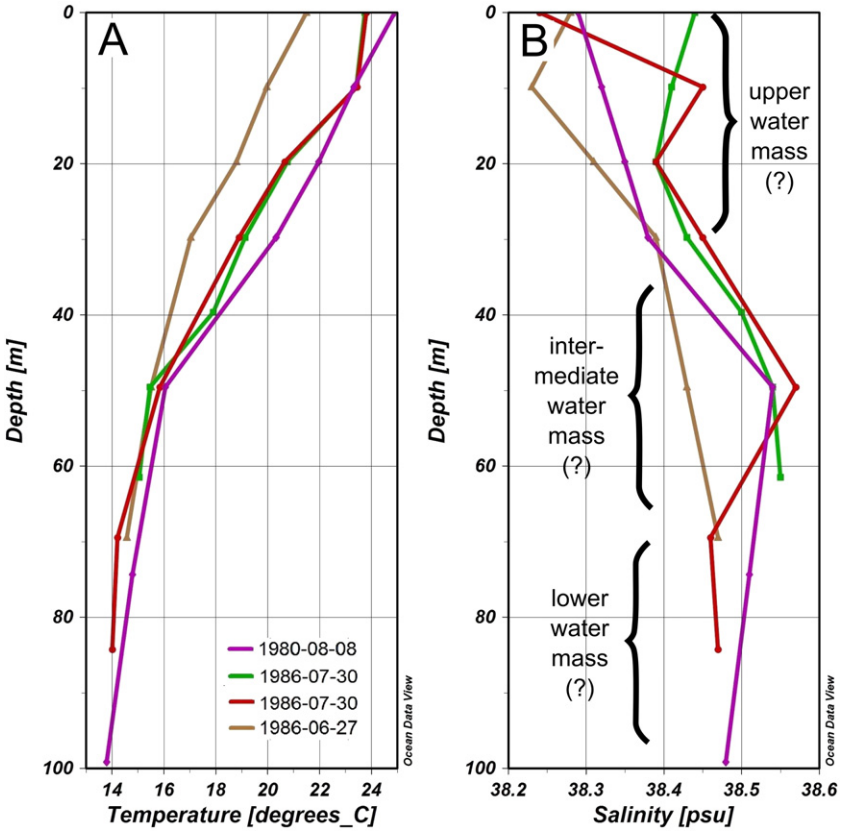

Fig. 14. A) temperature, B) salinity profiles in the center of the Nafpaktos Bay from the World Ocean Database (http://www.nodc.noaa.gov/). Plots correspond to station IDs 705, 823, 839 and 871 (see the World Ocean Database for their accurate locations).

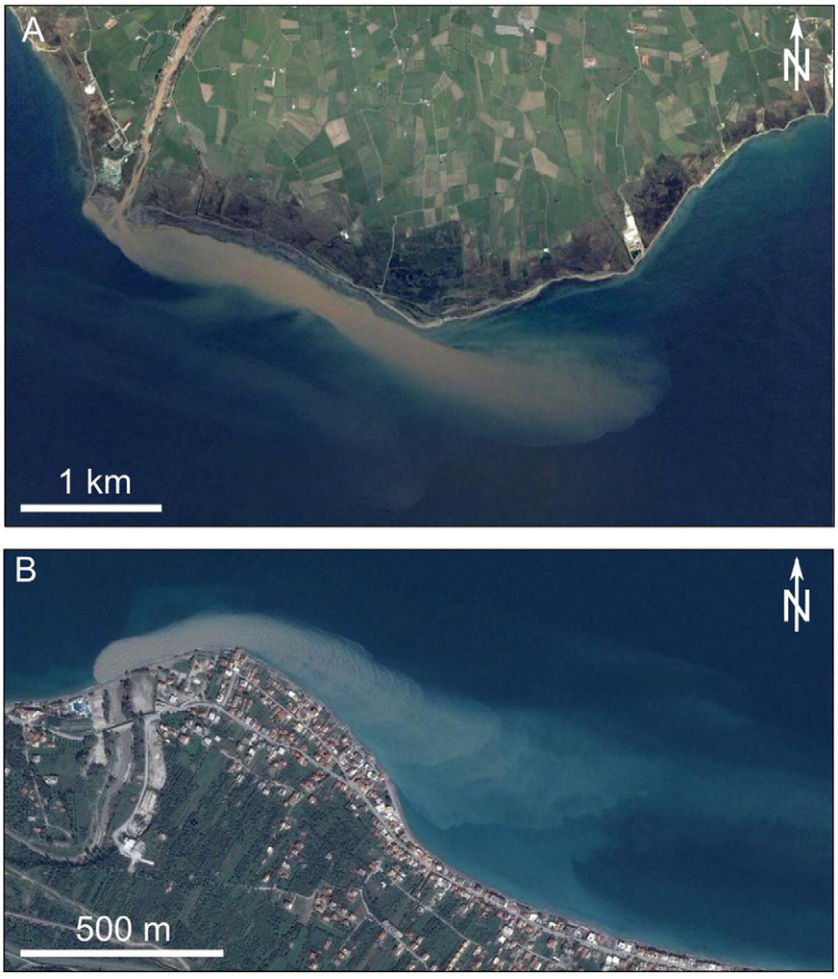

Fig. 15. Satellite imagery of river sediment plumes in the Gulf of Corinth deflected by marine currents. A) Mornos River, 27th March 2006; B) Fonissa River, 15th February 2014. Location of the river mouths in Fig. 1C. Source: Google Earth©.

The modern age of terrestrial organic matter sampled in this unit (younger than 1670 AD after calibration) indicates a recent age for U3, and consequently no significant recent seafloor erosion in this area. In comparison, the absence of U3 in NAF06 and NAF07, located in the deepest part of the Nafpaktos Bay, supports a more intense seafloor erosion in that area. Unit 2, which has been observed in the 3 cores (Fig. 5B and D), is interpreted as a transgressive deposit. The 14C dating of the *Turritella* sp. specimen in the Unit 1 below implies that the transgressive episode occurred after ~10 ka BP (uncalibrated and uncorrected from reservoir age). The clayey–silty, *Turritella* sp.-rich Unit 1 including thin dark sandy layers, interpreted as thin turbidites, would have been deposited in shallow-water (depth < 100 m) marine/lagoon environment, protected from bottom currents or swell. Indeed recent *Turritellidae* live in marine or brackish environments, most commonly in waters less than 100 m deep (Allmon, 1988).

The following link between the sedimentary units identified in these 3 cores and the morpho-sedimentary features highlighted in the seismic profiles is proposed. In the center of the Nafpaktos Bay, the transgressive sedimentary unit U2 could correspond to the "unconformity 1" identified locally around the furrow f3 (Fig. 5A). The 400 m-wide buried channel located in the same area (Fig. 5A) could also correspond to the same transgressive event, which would have occurred after ~10 ka BP (uncalibrated and uncorrected from reservoir age). The nature of this erosional event will be discussed in Section 6.1.

5.2. Other morpho-sedimentary features and related sedimentary processes

Besides bottom-current related features, there is a large variety of depositional environments in the study area: basin fill, draping on slopes, Gilbert-delta related deposits, MTDs and mounded structures. Results of this study allow proposing some new interpretations for two of them: the basin fill in the Mornos Canyon and the mounded structures.

5.2.1. The basin fill in the Mornos Canyon

In the Mornos Canyon, the Holocene infill imaged as high-amplitude reflections (Fig. 8A) is interpreted to represent fine-grained hemipelagites interbedded with coarser-grained sediment density flow deposits. This interpretation is supported by the core PSP05, which shows such an alternation in the central part of the Mornos Canyon (Fig. 8B). Two main sediment sources are proposed for the sediment density flow deposits recorded in the Mornos Canyon. First, at the western tip of the Mornos Canyon, the numerous gullies mapped on the eastern flank of the Mornos delta (Fig. 3A) suggest that at least some of these sediment density flows could have been turbidity currents resulting from sediment failures on the flanks of this delta. Then, south of the Mornos Canyon, the gullies located between the Erineos and Meganitis delta foresets, as well as the two MTDs located at the base of the Erineos prodelta slope highlight another sediment density flow origin, from the southern coast (Fig. 3A). Finally, we observed no gullies or channel connecting the deltas on the

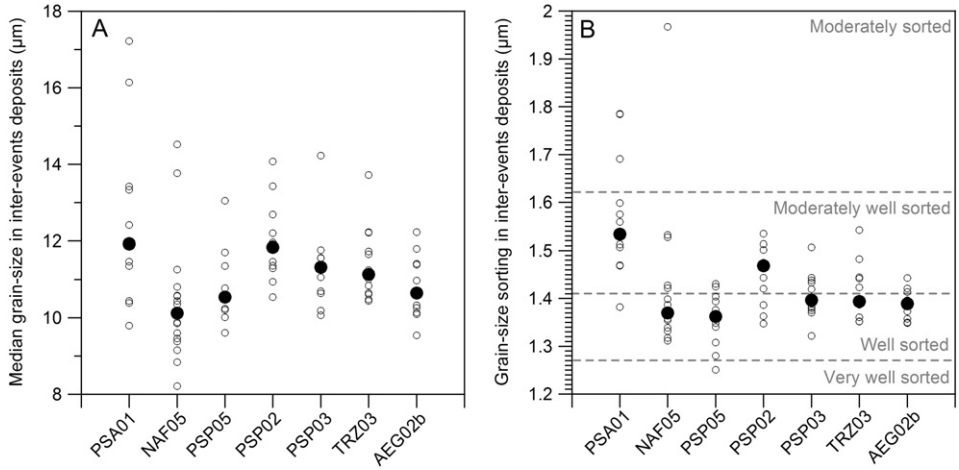

Fig. 16. Median grain-size (A) and sorting (B) for recent inter-event fine-grained sediments in 7 short cores from the western Gulf of Corinth. At least 10 samples have been measured in each core (circles). The black dots represent the median (left) or the mean (right) of all samples from each core. See Figs. 2 and 3 for core location.

northern coast (i.e. the Marathias and Sergoula River fan-deltas) to the Mornos Canyon. This suggests that the perched topography in the northern shelve traps most of the gravity flows that cannot reach the basin floor.

5.2.2. The mounded features

Farther east, seismic data have highlighted mounded features essentially located in the fan area of the Erineos prodelta (Fig. 3A). Two hypotheses are proposed for the genesis of these forms: (i) they could represent the summits of mud volcanoes caused by overpressure, or (ii) they may be large sediment blocks that failed from the steep delta foresets on the southern coast, e.g. the Erineos delta. The first mound, in Fig. 9B, is located in the center of a MTD that crops out at the seafloor, and has the same hummocky reflector pattern as the MTD. This would argue in favor of the sediment block hypothesis. In Fig. 9C, the second mound seems to result from the deformation of the upper sedimentary unit, rather than from a lateral advection of material at the surface. This is an indication that the mound may be a diapiric structure rather than a sediment block. Sedimentary loading due to rapid sedimentation (Dimitrov, 2002) is proposed as a possible driving force for this possible mud diapirism. Indeed, the thickness of Holocene sediments reaches 90 m in the foresets of the Erineos delta (Fig. 3B). This value is the highest value observed in our data in the study area. Such a sedimentary loading, associated with frequent seismic activity, is proposed to have remobilized under-compacted pre-Holocene MTDs that would have been deposited below the Erineos delta foresets. A last argument in favor of the diapiric origin is the spatial arrangement of the mounds. All are located in the gently dipping fan area, at a similar distance from the steep slopes of the Gilbert-type Erineos and Meganitis fan-deltas. This regularity is particularly clear from the 3D view of the seafloor in Lykousis et al. (2009) (their Fig. 5, p. 814) and is difficult to explain in the case of large rafted blocks, that are expected to travel along variable distances. Moreover, it seems likely that the specific conditions needed for the development of mud diapirs, i.e. high loading and the presence of liquefiable material, implies that mud diapirs are not distributed randomly. In summary, these observations are more favorable to the "mud volcanoes" hypothesis than to the "rafted blocks" hypothesis, for all the mounded structures.

5.3. Properties of drifted sediments compared to other deposits

Based on the sedimentary data from the cores presented above, we compared the sediment properties between muddy contourites sampled by the cores NAF05 and PSA01 on one hand to the background fine-grained sedimentation in other depositional environments on the other hand (cores PSP02, PSP03, PSP05, TRZ03 and AEG02b). The latter group of cores contains cores from "basin fill" (PSP05, TRZ03), "draping on slopes" (PSP03) and "shelf" (PSP02, AEG02b) environments. The aim was to identify some properties that can be used to discriminate muddy contourite from other kinds of fine-grained deposits (likely hemipelagites) in sediment cores.

5.3.1. Grain-size distribution, color and structure

Sediment color (gray-brown) and structure (almost no visible structure) are very similar in fine-grained interval of all the cores (cfr. the logs of the different cores in Figs. 5C, 7B and 8B). Regarding grain-size, the comparison of the D_{50} measured in the contourite drifts (cores PSA01 and NAF05) and in the muddy intervals of the other cores shows that grain size is very homogenous with a median grain-size between 8 and 15 µm (Fig. 16A). Only two samples from PSA01, in the southern drift, are lightly coarser-grained than the samples from the other coring sites (D_{50} of 16 and 17 µm, Fig. 16A). A slight difference in grain-size distribution between contourites and the other muddy deposits stands out from the comparison of sorting (Fig. 16B). Indeed, samples from PSA01 appear on average lightly less well sorted (higher Sorting Index) than samples from the other sites. Therefore, the recent contourites deposited on the drifts do not strongly differ from sediments that make up the background, likely hemipelagic, intervals in the other coring sites.

5.3.2. Magnetic properties

5.3.2.1. Median destructive field and characteristic remnant magnetization. In order to interpret the AMS measurements, it is first necessary to check that the measurements of the NRM can be used to estimate the orientation of the magnetic north in each core. This step is presented below based on the interpretation of the ranges of variations of the MDF, of the ChRM declination and of the ChRM inclination.

The range of values for the MDF between 20 and 40 mT suggests that the carrier of the remanence is ferrimagnetic, most likely magnetite (Fig. 11). The low variability of the MDF in each core also suggests that the carrier of the remanence in each core does not strongly vary with depth (Fig. 11). The inclination of the present geomagnetic field in the Gulf of Corinth area is about 54° (http://magnetic-declination.com). Assuming a possible inclination error of about 10° due to possible non-vertical coring, the ChRM inclination of TRZ03, PSP02 and PSA01 can consequently be considered as more or less normal (Table 1). Only the core PSP05 shows an average inclination value (33 ± 1.1°) that is different from the inclination of the present-day geomagnetic field. The range of variation of the declination in TRZ03, PSP02 and

PSA01 (~30°, not shown) is interpreted as reflecting, at least partially, the secular variations of the geomagnetic field that induced a shift of the declination of about 20° in the last 3 centuries, which is approximately the time span recorded in the studied cores (Beckers et al., 2013). This is not the case for PSP05, located in the Mornos Canyon, with only a shift of about 5° for the declination.

In summary, the data support that in TRZ03, PSP02 and PSA01, the ChRM orientation may correctly reflect the orientation of the geomagnetic field at the time of particle deposition. It is consequently proposed to use the average ChRM declination of each core to reorient ASM data regarding the magnetic north. For the core PSP05 in the Mornos Canyon, the ChRM declination and the ChRM inclination cannot be fully explained by a simple model assuming that only the geomagnetic field has controlled particles orientation. However, the ChRM is here used to roughly estimate the direction of the magnetic north at each coring site, rather than to accurately highlight past variations of the geomagnetic field. It is consequently proposed based on the presented results that the average ChRM declination deduced for the PSP05 site is also a reliable indication of the orientation of the magnetic north, but probably with a lower accuracy.

5.3.2.2. AMS parameters. The strong internal coherence between the K_{max} axes declination inside the six cores suggests that the grains are not randomly oriented at these coring sites (Fig. 12). It is proposed that bottom currents are responsible for this alignment of K_{max} axes in the contourites, as well as in the muddy sediments in the other coring sites, interpreted as hemipelagites according to their seismic facies. Moreover, concerning the cores from "basin fill" (PSP05 and TRZ03) and "shelf" environments (PSP02 and AEG02b), the similarity between AMS ellipsoids of samples from the fine-grained intervals and from sandy layers (Fig. 12) suggests that bottom currents also influence the orientation of the grains transported and deposited by sediment density flows. This is especially the case in PSP05, where the sandy layers are up to 4 cm thick and consequently fully fill the cubes used for the sampling.

The geographic orientation of the K_{max} axes is another parameter that can provide information about a possible influence of bottom currents on depositional processes. The K_{max} axes often are assumed to be parallel to the current direction. However, if the seafloor is not horizontal, grains can roll on the seafloor by gravity so that the K_{max} orientation is controlled by the slope direction (K_{max} parallel to the isobaths). In the sub-basin west of the Trizonia Island (core TRZ03), average K_{max} orientation is parallel to the isobaths. This orientation of the grains may result from gravity-induced rolling or contour-parallel bottom currents. In the Mornos Canyon (core PSP05), the K_{max} orientation follow the canyon axis and suggests the existence of a bottom current oriented in this direction. Turbidity currents could be invoked as well (e.g. Shor et al., 1984), but the fact that all samples show the same K_{max} orientation whatever the sedimentary unit they come from (fine-grained "background" intervals or sandy event deposits) suggests a continuous process, such as bottom-currents, rather than occasional turbidity currents. In the southern sediment drift (PSA01), K_{max} orientation makes an angle of about 60° with the isobaths, which also suggests a possible influence of west–east bottom currents. Finally, in the Erineos delta area (PSP02), the seafloor relief is not well constrained so that the comparison between the orientation of the isobaths and the orientation of the K_{max} axes is not possible.

6. Discussion

The western tip of the Gulf of Corinth shows a large diversity of depositional and erosional features, in a relatively small area. These features result from the interaction of different sedimentary processes, which are discussed hereafter Section 6.1. In Section 6.2, different aspects linked to the existence of shallow water sediment drifts in the Gulf of Corinth are discussed, based on the interpretations presented above combined with results from the literature. Finally, Section 6.3 summarizes the data that are available for a better understanding of the water circulation pattern in the Gulf of Corinth.

6.1. Sedimentary processes and their timing at the western tip of the Gulf of Corinth

Different sedimentary processes are proposed to be active at the western tip of the Gulf of Corinth, between the Rion and the Mornos–Drepano sills. Currents divert river plumes (over- or interflows) and allow the building of shallow-water sediment drifts around the Drepano delta and on the margins of the Nafpaktos Bay (northern and southern sediment drifts). Besides, currents are eroding the bottom of the Nafpaktos Bay, the Mornos–Drepano sill, and the base of the drifts. Secondary helical circulations in the Nafpaktos Bay induce the formation of furrows (Fig. 4). East of the Mornos–Drepano sill, scarps possibly related to submarine landsliding (see our arguments in Section 6.2.3.) are reworked by bottom currents, and scours form at the foot of the scarp (Fig. 6). Downslope, another sediment drift develops and is laterally connected to the southern drift (Fig. 6). The absence of sediment drift on the southeastern flank of the Mornos delta would result from its location in the axis of the Nafpaktos Bay that would orient the currents along the Mornos delta foresets, preventing the deposition of relatively fine-grained sediments. The frequent submarine landslides that affect the delta foresets also contribute to the absence of sediment drift at this location. East of the Mornos–Drepano sill, gravitational processes such as submarine landslides and turbidity currents seem to play a larger role in sediment transport than bottom currents, as proposed by Ferentinos et al. (1988) and Lykousis et al. (2007a). However, the specific magnetic fabric highlighted in the Trizonia sub-basin, in the Mornos Canyon and in the Erineos and Aigion shelves (Fig. 12) suggests that bottom currents influence the sedimentation in various places of the western Gulf of Corinth by reorienting the grains during or shortly after their deposition. The directions of the K_{max} axes in the Trizonia sub-basin and in the Erineos Shelf (Fig. 13) also support the existence of contour-parallel bottom currents in these areas.

Moreover, data collected in the Nafpaktos Bay provide new information about the connection of the Corinth Lake and the adjacent Gulf of Patras area with the Mediterranean Sea during the last sea level rise. In the center of the Nafpaktos Bay, below 10 to 20 m of sediments, an unconformity has been correlated to a transgression surface that is well imaged in the northern part of the Bay (Fig. 5A; Fig. 7 in Beckers et al., 2015). This onlap surface clearly reflects an increase in the water level, and probably corresponds to the transition between a non-marine and a marine environment that has been dated at ca. 12 ka BP at the eastern tip of the Gulf (Collier et al., 2000). A younger transgressive unit, up to 1.2 m thick, is observed in the three cores retrieved in the center of the Bay (sedimentary unit U2, Fig. 5B and D), as well as in high-resolution seismic profiles (seismic unconformity 1, Fig. 5A). U2 locally crops out in the sea bottom and has a basal age of 10.2 ka BP (uncalibrated) according to the new radiocarbon age presented in this study. A wide paleo-channel is observed in the seismic lines close to the location of those cores (Fig. 5A). It could result from the same transgressive event as U2. Consequently, our results suggest that the last transgression occurred in two different pulses in the Nafpaktos Bay. A first phase would have occurred at ca. 12 ka BP (uncalibrated, from Collier et al., 2000), while a second phase would have deposited U2 after 10.2 ka BP (uncalibrated, this study). It is proposed that after the first pulse at ca. 12 ka BP, fine-grained sediments (U1) accumulated in the Bay at a sufficient rate to maintain a shallow water environment. Then, an increase in the rate of relative sea level rise would have been responsible for the second transgressive pulse observed in the Nafpaktos Bay (U2). The ongoing sea level rise finally reached a sufficient elevation above the Acheloos–Cape Pappas sill (which is 50–55 m deep if the Holocene surface veneer of sediment is subtracted from the present depth, Fig. 1B) and the Rion sill (62 m deep), so a complete marine connection occurred and the sediment drifts started to

develop after 8–9 ka BP. The later interpretation is also in agreement with sedimentological record in the middle of the Gulf sampling the Lacustrine–Marine transition (Moretti et al., 2004). The first marine influx is attested by the precipitation of aragonite needles (Van Welden, 2007) and occurred at ca. 11.3 ka BP (uncalibrated age derived from Campos et al., 2013a). The full connection and the establishment of the present sedimentological regime occurred later, around 10.4 ka BP (Campos et al., 2013a), and is marked by an increase in magnetic susceptibility and the occurrence of frequent turbiditic flows (Van Welden, 2007).

6.2. Contourite characteristics

6.2.1. Possible sediment sources

Sedimentological characteristics of the Gulf of Corinth contourites are very similar to the fine-grained sediments interpreted as hemipelagites in the coring sites east of the drifts. This suggests that the sediment sources of the drifts are local river sediment plumes, i.e. the Mornos and the Drepano rivers. River plumes in this area are sometimes strongly deflected by currents (Fig. 15). Moreover, in the time scale of the Holocene, the thickness of the southern sediment drift is larger east of the Drepano River delta than west of this delta, in the Nafpaktos Bay. This asymmetry consequently suggests that the net sediment transport is oriented toward the east. Apart from the direct input from river sediment plumes (distributed as overflows or interflows), the possibility that sediments eroded in the center of the Nafpaktos Bay contribute to the sediment accumulation on the drifts cannot be ruled out.

6.2.2. Diagnostic criteria

Apart from the typical shape of the sediment drift depositional reliefs, the criteria proposed here to discriminate contourites from other fine-grained deposits in the Gulf of Corinth environment are the high homogeneity under X-rays, the higher AMS (higher value of P, Table 2), and, for some samples from the core PSA01, a weaker grain-size sorting (Fig. 16). A higher sorting (i.e. lower Sorting Index, close to 1) was expected for the drift sediments compared to “classical” hemipelagites. This counterintuitive value for the sorting may result from the proximal location of the core PSA01 regarding the Drepano River mouth (Fig. 4A). Indeed, if the sediment sources of the drifts are the local river plumes, as it is proposed, then river discharge fluctuations during floods may weaken the sorting of sediments deposited near the river mouth. Furthermore, the likely strong variability in current strength through time in the Nafpaktos Bay may also lead toward a weaker sorting in the sediment drifts compared to “classical” hemipelagites. Based on these criteria, the identification of similar shallow-water muddy sediment drifts in the ancient records can provide indications on the paleogeography of the system. For example, looking for similar sediment drifts in exhumed rift sediments, such as those covering the north of the Peloponnese, may give indications on ancient water depth, bottom currents, and on a possible connection to the open sea.

6.2.3. Comparison with other sediment drifts

According to recent classifications of sediment drifts, the northern and southern sediment drifts located in the Nafpaktos Bay belong to the “plastered drifts”, which develop in deep oceans on gentle slopes swept by relatively low-velocity currents (e.g. Hernandez-Molina et al., 2003; Rebesco et al., 2014; Pérez et al., 2015). Comparing the sedimentary features identified in this study to bottom-current related erosional and depositional features described elsewhere helps to distinguish the effects of bottom currents from those of gravity-driven processes, and also gives us an idea about the type of circulation pattern that could be responsible for the formation of the sediment drifts in the Gulf of Corinth.

In this way, the curved scarp located just east of the Mornos–Drepano sill and the sediment drift located downslope (eastern tip of the southern sediment drift, Fig. 6) are similar to morphologies described in the SW Adriatic margin (Verdicchio and Trincardi, 2008b, e.g. their Fig. 4). These authors interpret seaward-concave moats in a shelf-edge area to initially result from sediment failure, reworked afterward by bottom currents flowing parallel or oblique to the depth contours. Considering the numerous slope failures and MTDs located north and west of the Mornos–Drepano sill, it is proposed that the same model may hold for this area, i.e. that the curved scarp initially results from landsliding and has been subsequently reshaped by bottom currents.

The northern and southern sediment drifts identified in the Nafpaktos Bay on both sides of the Gulf axis show similarities to drifts described in the Gulf of Izmit, Sea of Marmara (Kuscu et al., 2002). The two gulfs have a similar shape and comparable widths and depths, so it is relevant to compare both systems. The oceanography of the Gulf of Izmit is better known than that of the Gulf of Corinth. It has a permanent two-layered water system connected to the water circulation of the Sea of Marmara (Balkis, 2012). The upper layer consists of less saline water from the Black Sea, while the lower layer originates from the Mediterranean Sea. The two layers flow in different directions depending on the season, and are probably responsible for the establishment of the drifts. In the Gulf of Corinth, it is unlikely that the bottom currents are driven by such strong thermohaline gradients. Indeed, published CTD data does not highlight any permanent change in water temperature or salinity along vertical profiles that could be interpreted as a simple and permanent thermohaline circulation (Poulos et al., 1996).

Finally, a similar comparison can be done with plastered drifts in the Alboran Sea, east of the Strait of Gibraltar (Ercilla et al., 2015). There, the morphology of plastered drifts located on the Spanish and the Moroccan slopes is also very similar to the one of the drifts presented in this study. Their geometry has been explained by the near-bottom layer distribution of the Mediterranean water-masses bounded by the most pronounced density contrasts (Ercilla et al., 2015). Although the spatial scales differ between the Gulf of Corinth and the Alboran Sea, this suggests that the water circulation at the entrance of the Gulf of Corinth also involves superimposed water-masses with different densities and that such a circulation, permanent or not, governs the general physiography.

6.3. Possible circulation patterns and mechanisms for the currents at the entrance of the Gulf of Corinth

The morphology of the Gulf of Corinth is somewhat similar to the one of a fjord, with a deep depression connected to the open sea through a shallow sill. The typical water circulation in a fjord consists in a brackish outflow on the surface above a deeper compensation current (Farmer and Freeland, 1983). Besides this simple mechanism, other processes can contribute to the water circulation such as tides, winds, and turbulence. By combining the results of this study with previous works, it is possible to propose some hypothesis about the circulation pattern at the entrance of the Gulf of Corinth that could explain the presence of sediment drifts, and to discuss the influence of the possible driving mechanisms. Despite the low tidal range in the Mediterranean Sea (average mean tidal range of 15 cm for the Gulf of Corinth, Tsimplis, 1995), models show that tides are responsible for strong currents in the Rion Straits exceeding 1 m s^{-1} (Fourniotis and Horsch, 2010, 2012). This velocity is sufficient to erode and transport silt- and sand-size particles (Hjulstrom, 1935). Tidal currents can consequently be invoked for the transport and the deposition of the silt-size particles from the sediment drifts. Because the Gulf of Corinth is closed at its eastern tip, the existence of tidal currents in the Rion Straits area implies that a secondary current flows simultaneously in the opposite direction. Fourniotis and Horsch's (2012) modeling study suggests that during summer flood tide conditions an upper current flows toward the Gulf of Corinth on top of a stronger bottom current flowing toward the west. Such a two layers model fits with the eastward deviation of the Mornos and the Fonissa

rivers sediment plumes observed on satellite images in March 2006 and in February 2014, respectively (Fig. 15).

This simple two layer circulation model is challenged by CTD profiles acquired between June and August in the Nafpaktos Bay. The CTD shows a slight increase in salinity at −50 m (Fig. 14B), suggesting more complicated water stratification in this area with possibly 3 different water masses during summer time. Similar increase in salinity has been observed between −125 m and −175 m in the Gulf of Corinth and has been interpreted as an input of the more saline Ionian Sea waters over the Rion sill (Anderson and Carmack, 1973; in Poulos et al., 1996). This interpretation supports the occurrence of a three layer flow in the Nafpaktos Bay, the intermediate one flowing toward the Gulf of Corinth (at 30–70 m bsl) while the upper and the lower water masses (at 0–30 and 70–115 m bsl) would flow in the opposite direction (Fig. 14B). This more complex circulation pattern during summer time is not incompatible with a two layers circulation during the other periods that is responsible for the river plume deflection.

Finally, the inferred strong turbulence that occurs at the entrance of the Gulf of Corinth, in the Nafpaktos Bay, must disturb a two or three layer circulation pattern. The particular conditions leading to turbulence need to be further studied. Similarly, the presence of north–south trending scours in the eastern slope of the Mornos–Drepano sill (Fig. 6) also suggests the occurrence of turbulent flow or lee waves in this area. Such flow behavior could result from the abrupt increase in water depth east of the sill (e.g. Farmer and Freeland, 1983).

In summary, a definitive circulation model at the entrance of the Gulf of Corinth cannot be established with the present data that represents different time-scales. Sedimentological observations give indications about the average conditions during the last few thousand years, while the modeling exercises in the Gulf of Patras (Fourniotis and Horsch, 2012), satellite images from the Gulf of Corinth (this study) and CTD profiles represent specific conditions in terms of tide, wind, surface temperature, etc. Seasonal variations in tidal amplitudes, winds and water density gradients between the Gulf of Corinth and the Ionian Sea are not well constrained and would influence the circulation pattern. Continuous long term current meter measurements are necessary to understand the complexity of the flow pattern.

7. Conclusion

A dense grid of high-resolution seismic profiles reveals the existence of shallow-water sediment drifts in the Gulf of Corinth. The drifts developed at the entrance of the Gulf during the Holocene mainly on both sides whereas various erosional bedforms are documented in its central part. The thickness of the drifts reaches at least 50 m and coring indicates that drifts are composed of homogenous bioturbated mud in their upper part. A comparison between sediments sampled in the drift and fine-grained sediments sampled at different locations in the Western Gulf of Corinth shows that recent contourites and hemipelagites have similar properties in terms of color, structure, grain size distribution and magnetic fabric. The magnetic fabric suggests an influence of bottom currents on grains orientation in the drift, and also in the deposits initially interpreted as hemipelagites. The presented data highlight the difficulty to identify ancient sediment drifts in outcrops. In rifted margins, such as in the Corinth Rift, looking for similar depositional sequences with similar magnetic fabric in the uplifted synrift series may provide useful information about ancient water depths and about a possible water connection between the basins and the sea.

Acknowledgments

The ANR (France, SISCOR project) and the FNRS (Belgium, "*Ruptures sismiques du Rift de Corinthe*" project) provided financial supports for the field surveys. Many thanks to Koen De Rycker for the seismic acquisition and to the students of the Laboratory of Marine Geology and Physical Oceanography, University of Patras, for their participation in the 2014 coring campaign. We warmly thank the R/V Alkyon and R/V Eleni crews for the seismic and coring surveys in 2011, 2012 and 2014 and Pascale Bascou for technical support. David Van Rooij and Simo Spassov have provided useful comments during the preparation of this manuscript. We thank N. Thouveny (CEREGE — Aix Marseille University) for giving us access to magnetic facilities. In addition, F. Demory (CEREGE) and the Geophysical Center of Dourbes are acknowledged for the magnetic measurements. Arnaud Beckers PhD grant was supported by the Belgian FRIA. Finally, we thank N. Cagatay and an anonymous reviewer for their constructive remarks that largely improved the content of this paper.

References

Allmon, W.D., 1988. Ecology of Recent turritelline gastropods (Prosobranchia, Turritellidae): current knowledge and paleontological implications. PALAIOS 3, 259–284. http://dx.doi.org/10.2307/3514657.

Anderson, J.J., Carmack, E.C., 1973. Some physical and chemical properties of the Gulf of Corinth. Estuar. Coast. Mar. Sci. 1, 195–202.

Baas, J.H., Hailwood, E.a., McCaffrey, W.D., Kay, M., Jones, R., 2007. Directional petrological characterisation of deep-marine sandstones using grain fabric and permeability anisotropy: methodologies, theory, application and suggestions for integration. Earth-Sci. Rev. 82, 101–142. http://dx.doi.org/10.1016/j.earscirev.2007.02.003.

Balkis, N., 2012. The effect of Marmara (Izmit) earthquake on the chemical oceanography and Mangan enrichment in the lower layer. In: D'Amico, S. (Ed.), Statistical Studies, Observations and Planning. inTech.

Beckers, A., Mortier, C., Beck, C., Hubert-Ferrari, A., Reyss, J., Tripsanas, E., Sakelariou, D., De Batist, M., De Rijcker, K., Bascou, P., Strivay, D., 2013. High energy environment offshore deposits in the western Gulf of Corinth, Greece. European Geoscience Union General Assembly Abstracts (Vienna).

Beckers, A., Hubert-Ferrari, A., Beck, C., Bodeux, S., Tripsanas, E., Sakellariou, D., De Batist, M., 2015. Active faulting at the western tip of the Gulf of Corinth, Greece, from high-resolution seismic data. Mar. Geol.

Bell, R.E., McNeill, L.C., Bull, J.M., Henstock, T.J., 2008. Evolution of the offshore western Gulf of Corinth. Geol. Soc. Am. Bull. 120, 156–178. http://dx.doi.org/10.1130/B26212.1.

Bell, R.E., McNeill, L.C., Bull, J.M., Henstock, T.J., Collier, R.E.L., Leeder, M.R., 2009. Fault architecture, basin structure and evolution of the Gulf of Corinth Rift, Central Greece. Basin Res. 21, 824–855. http://dx.doi.org/10.1111/j.1365-2117.2009.00401.x.

Blott, S.J., Pye, K., 2001. Gradistat : a grain size distribution and statistics package for the analysis of unconsolidated sediments. Earth Surf. Process. Landf. 26, 1237–1248.

Campos, C., Beck, C., Crouzet, C., Carrillo, E., Welden, A. Van, Tripsanas, E., 2013a. Late Quaternary paleoseismic sedimentary archive from deep central Gulf of Corinth : time distribution of inferred earthquake-induced layers. Ann. Geophys. 56, 1–15. http://dx.doi.org/10.4401/ag-6226.

Campos, C., Beck, C., Crouzet, C., Demory, F., Van Welden, A., Eris, K., 2013b. Deciphering hemipelagites from homogenites through anisotropy of magnetic susceptibility. Paleoseismic implications (Sea of Marmara and Gulf of Corinth). Sediment. Geol. 292, 1–14. http://dx.doi.org/10.1016/j.sedgeo.2013.03.015.

Charalampakis, M., Lykousis, V., Sakellariou, D., Papatheodorou, G., Ferentinos, G., 2014. The tectono-sedimentary evolution of the Lechaion Gulf, the south eastern branch of the Corinth graben, Greece. Mar. Geol. 351, 58–75. http://dx.doi.org/10.1016/j.margeo.2014.03.014.

Collier, R.E.L., Leeder, M.R., Trout, M., Ferentinos, G., Lyberis, E., Papatheodorou, G., 2000. High sediment yields and cool, wet winters : test of last glacial paleoclimates in the northern Mediterranean. Geology 28, 999–1002. http://dx.doi.org/10.1130/0091-7613(2000)28<999.

Cotterill, C.J., 2006. A High-resolution Holocene Fault Activity History of the Aigion Shelf, Gulf of Corinth, Greece (PhD Thesis) University of Southampton.

Dall'olio, E., Felletti, F., Muttoni, G., 2013. Magnetic-fabric analysis as a tool to constrain mechanisms of deep-water mudstone deposition in the Marnoso Arenacea Formation (Miocene, Italy). J. Sediment. Res. 83, 170–182. http://dx.doi.org/10.2110/jsr.2013.12.

Dimitrov, L.I., 2002. Mud volcanoes—the most important pathway for degassing deeply buried sediments. Earth-Sci. Rev. 59, 49–76. http://dx.doi.org/10.1016/S0012-8252(02)00069-7.

Ellwood, B.B., 1980. Application of the anisotropy of magnetic susceptibility method as an indicator of bottom-water flow direction. Mar. Geol. 34, M83–M90. http://dx.doi.org/10.1016/0025-3227(80)90066-3.

Ellwood, B.B., Ledbetter, M.T., 1977. Antarctic bottom water fluctuations in the Vema Channel: effects of velocity changes on particle alignment and size. Earth Planet. Sci. Lett. 35, 189–198. http://dx.doi.org/10.1016/0012-821X(77)90121-2.

Ercilla, G., Juan, C., Hernández-Molina, J., Bruno, M., Estrada, F., Alonso, B., Casas, D., Farran, M., Llave, E., García, M., Vázquez, J., D'Acremont, E., Gorini, C., Palomino, D., Valencia, J., El Moumni, B., Ammar, A., 2015. Significance of Bottom Currents in Deep-sea Morphodynamics: An Example from the Alboran Sea, Marine Geology, Available Online 16 September 2015 (ISSN 0025–3227).

Farmer, D.M., Freeland, H.J., 1983. The physical oceanography of fjords. Prog. Oceanogr. 12, 147–220. http://dx.doi.org/10.1016/0079-6611(83)90004-6.

Ferentinos, G., Papatheodorou, G., Collins, M.B., 1988. Sediment transport processes on an active submarine fault escarpment: Gulf of Corinth, Greece. Mar. Geol. 83, 43–61. http://dx.doi.org/10.1016/0025-3227(88)90051-5.

Flood, R.D., 1983. Classification of sedimentary furrows and a model for furrow initiation and evolution. Geol. Soc. Am. Bull. 94, 630–639.

Flood, R.D., Kent, D.V., Shor, A.N., Hall, F.R., 1985. The magnetic fabric of surficial deep-sea sediments in the HEBBLE area (Nova Scotian continental rise). Mar. Geol. 66, 149–167. http://dx.doi.org/10.1016/0025-3227(85)90027-1.

Ford, M., Williams, E.A., Malartre, F., Popescu, S., 2009. Stratigraphic architecture, sedimentology and structure of the Vouraikos Gilbert-type fan delta, Gulf of Corinth, Greece. In: Nichols, G., Williams, E., Paola, C. (Eds.), Sedimentary Processes, Environments and Basins: A Tribute to Peter Friend. Blackwell Publishing Ltd., Oxford.
Ford, M., Rohais, S., Williams, E.a., Bourlange, S., Jousselin, D., Backert, N., Malartre, F., 2013. Tectono-sedimentary evolution of the Western Corinth Rift (Central Greece). Basin Res. 25, 3–25. http://dx.doi.org/10.1111/j.1365-2117.2012.00550.x.
Fourniotis, N.T., Horsch, G.M., 2010. Three-dimensional numerical simulation of wind-induced barotropic circulation in the Gulf of Patras. Ocean Eng. 37, 355–364. http://dx.doi.org/10.1016/j.oceaneng.2010.01.002.
Fourniotis, N.T., Horsch, G.M., 2012. Early summer circulation in the Gulf of Patras (Greece). Isope 4, 740–745.
Galanopoulos, A., Delimbasis, N.D., Comninakis, P.E., 1964. A tsunami generated by a slide without a seismic shock. Geol. Chron. Greece 16, 93–110.
Hamilton, N., Rees, A.I., 1970. Magnetic fabric of sediments from the shelf at La Jolla (California). Mar. Geol. 9, M6–M11. http://dx.doi.org/10.1016/0025-3227(70)90060-5.
Heezen, B.C., Ewing, M., Johnson, G.L., 1966. The Gulf of Corinth floor. Deep Res. 13, 381–411.
Hellenic Hydrographic Service, 1984. Pilot.
Hernandez-Molina, J., Llave, E., Fernandez-Puga, M.C., Maestro, A., Leon, R., Medialdea, T., Barnolas, A., Garcia, M., del Rio, V.D., Fernandez-Salas, L.M., Vazquez, J.T., Lobo, F., Alveirinho Dias, J., Rodero, J., Gardner, J., 2003. Looking for clues to paleoceanographic imprints : a diagnosis of the Gulf of Cadiz contourite depositional systems. Geology 31, 19–22.
Hext, G.R., 1963. The estimation of second-order tensors, with related tests and designs. Biometrika 50, 353–373.
Hjulstrom, F., 1935. The morphological activity of rivers as illustrated by River Fyris. Bull. Geol. Inst. 25.
Kuscu, I., Okamura, M., Matsuoka, H., Awata, Y., 2002. Active faults in the Gulf of Izmit on the North Anatolian Fault, NW Turkey: a high-resolution shallow seismic study. Mar. Geol. 190, 441–443.
Lascaratos, A., Salusti, E., Papageorgaki, G., 1989. Wind-induced upwellings and currents in the gulfs of Patras, Nafpaktos and Korinthos, Western Greece. Oceanol. Acta 12, 159–164.
Ledbetter, M.T., Ellwood, B.B., 1980. Spatial and temporal changes in bottom-water velocity and direction from analysis of particle size and alignment in deep-sea sediment. Mar. Geol. 38, 245–261.
Lemeille, F., Chatoupis, F., Foumelis, M., Rettenmaier, D., Unkel, I., Micarelli, L., Moretti, I., Bourdillon, C., Guernet, C., Müller, C., 2004. Recent syn-rift deposits in the hangingwall of the Aigion Fault (Gulf of Corinth, Greece). Compt. Rendus Geosci. 336, 425–434. http://dx.doi.org/10.1016/j.crte.2003.11.009.
Lurcock, P.C., Wilson, G.S., 2012. PuffinPlot: a versatile, user-friendly program for paleomagnetic analysis. Geochem. Geophys. Geosyst. 13, 1–6. http://dx.doi.org/10.1029/2012GC004098.
Lykousis, V., 1990. Prodelta sediments: seismic stratigraphy, sedimentology, slope stability (PhD Thesis) University of Patras.
Lykousis, V., Karageorgis, A.P., Chronis, G.T., 2005. Delta progradation and sediment fluxes since the last glacial in the Thermaikos Gulf and the Sporades Basin, NW Aegean Sea, Greece. Mar. Geol. 222–223, 381–397. http://dx.doi.org/10.1016/j.margeo.2005.06.026.
Lykousis, V., Sakellariou, D., Moretti, I., Kaberi, H., 2007a. Late Quaternary basin evolution of the Gulf of Corinth: sequence stratigraphy, sedimentation, fault–slip and subsidence rates. Tectonophysics 440, 29–51. http://dx.doi.org/10.1016/j.tecto.2006.11.007.
Lykousis, V., Sakellariou, D., Rousakis, G., Alexandri, S., Kaberi, H., Nomikou, P., Georgiou, P., Balas, D., 2007b. Sediment failure processes in active grabens: the western Gulf of Corinth (Greece). In: Lykousis, V., Sakellariou, D., Locat, J. (Eds.), Submarine Mass Movements and Their Consequences III. Springer, pp. 297–305.
Lykousis, V., Roussakis, G., Sakellariou, D., 2009. Slope failures and stability analysis of shallow water prodeltas in the active margins of Western Greece, northeastern Mediterranean Sea. Int. J. Earth Sci. 98, 807–822. http://dx.doi.org/10.1007/s00531-008-0329-9.
Moretti, I., Lykousis, V., Sakellariou, D., Reynaud, J.-Y., Benziane, B., Prinzhoffer, A., 2004. Sedimentation and subsidence rate in the Gulf of Corinth: what we learn from the Marion Dufresne's long-piston coring. Compt. Rendus Geosci. 336, 291–299. http://dx.doi.org/10.1016/j.crte.2003.11.011.
Ori, G., 1989. Geologic history of the extensional basin of the Gulf of Corinth (? Miocene–Pleistocene), Greece. Geology 17, 918–921. http://dx.doi.org/10.1130/0091-7613(1989)017<0918.
Papatheodorou, G., Ferentinos, G., 1997. Submarine and coastal sediment failure triggered by the 1995, M = 6.1 R Aegion earthquake, Gulf of Corinth, Greece. Mar. Geol. 137, 287–304.
Papatheodorou, G., Stefatos, A., Christodoulou, D., Ferentinos, G., 2003. Small scale present day turbidity currents in a tectonically active submarine graben, the Gulf of Corinth (Greece): their significance in dispersing mine tailings and their relevance to basin filling. In: Locat, J., Mienert, J. (Eds.), Submarine Mass Movements and Their Consequences, Advances in Natural and Technological Hazards Research. Kluwer Academic, Dordrecht, pp. 459–468 http://dx.doi.org/10.1007/978-94-010-0093-2.
Parés, J.M., Hassold, N.J.C., Rea, D.K., van der Pluijm, B.A., 2007. Paleocurrent directions from paleomagnetic reorientation of magnetic fabrics in deep-sea sediments at the Antarctic Peninsula Pacific margin (ODP Sites 1095, 1101). Mar. Geol. 242, 261–269. http://dx.doi.org/10.1016/j.margeo.2007.04.002.
Pérez, L.F., Hernández-Molina, F.J., Esteban, F.D., Tassone, A., Piola, A.R., Maldonado, A., Preu, B., Violante, R.a., Lodolo, E., 2015. Erosional and depositional contourite features at the transition between the western Scotia Sea and southern South Atlantic Ocean: links with regional water-mass circulation since the Middle Miocene. Geo-Mar. Lett. 35, 271–288. http://dx.doi.org/10.1007/s00367-015-0406-6.
Perissoratis, C., Piper, D.J.W., Lykousis, V., 2000. Alternating marine and lacustrine sedimentation during late Quaternary in the Gulf of Corinth Rift basin, central Greece. Mar. Geol. 167, 391–411.
Piper, D.J.W., Kontopoulos, N., Panagos, A.G., 1988. Deltaic sedimentation and stratigraphic sequences in post-orogenic basins, Western Greece. Sediment. Geol. http://dx.doi.org/10.1016/0037-0738(88)90135-2.
Piper, D.J.W., Kontopoulos, N., Anagnostou, C., Chronis, G., Panagos, A.G., 1990. Modern fan deltas in the western Gulf of Corinth, Greece. Geo-Mar. Lett. 10, 5–12.
Poulos, S.E., Collins, M.B., Pattiaratchi, C., Cramp, A., Gull, W., Tsimplis, M., Papatheodorou, G., 1996. Oceanography and sedimentation in the semi-enclosed, deep-water Gulf of Corinth (Greece). Mar. Geol. 134, 213–235. http://dx.doi.org/10.1016/0025-3227(96)00028-X.
Rebesco, M., Hernández-Molina, F.J., Van Rooij, D., Wåhlin, A., 2014. Contourites and associated sediments controlled by deep-water circulation processes: state-of-the-art and future considerations. Mar. Geol. 352, 111–154. http://dx.doi.org/10.1016/j.margeo.2014.03.011.
Rees, A.I., 1961. The effect of water currents on the magnetic remanence and anisotropy of susceptibility of some sediments. Geophys. J. R. Astron. Soc. 5, 235–251. http://dx.doi.org/10.1111/j.1365-246X.1961.tb00431.x.
Schlitzer, R., 2015. Ocean Data View.
Schwartz, M., Tziavos, C., 1979. Geology in the search for ancient Helice. J. Field Archaeol. 6, 243–252.
Shor, A.N., Kent, D.V., Flood, R.D., 1984. Contourite or turbidite?: Magnetic fabric of fine-grained Quaternary sediments, Nova Scotia continental rise. Geol. Soc. Lond. Spec. Publ. 15, 257–273. http://dx.doi.org/10.1144/GSL.SP.1984.015.01.17.
Siddall, M., Rohling, E., Almogi-Labin, A., Hemleben, C., Meischner, D., Schmelzer, I., Smeed, D.A., 2003. Sea-level fluctuations during the last glacial cycle. Nature 423, 19–24. http://dx.doi.org/10.1038/nature01687.1.
Singsoupho, S., Bhongsuwan, T., Elming, S.-Å., 2015. Palaeocurrent direction estimated in Mesozoic redbeds of the Khorat Plateau, Lao PDR, Indochina Block using anisotropy of magnetic susceptibility. J. Asian Earth Sci. http://dx.doi.org/10.1016/j.jseaes.2015.02.026.
Sivkov, V., Gorbatsky, V., Kuleshov, A., Zhurov, Y., 2002. Muddy contourites in the Baltic Sea: an example of a shallow-water contourite system. In: Stow, D.A.V., Pudsey, C.J., Howe, J.A., Faugères, J.-C., Viana, A.R. (Eds.), Deep-Water Contourite Systems: Modern Drifts and Ancient Series. Seismic and Sedimentary Characteristics, London, pp. 121–136.
Stefatos, A., Papatheodorou, G., Ferentinos, G., Leeder, M., Collier, R., 2002. Seismic reflection imaging of active offshore faults in the Gulf of Corinth: their seismotectonic significance. Basin Res. 14, 487–502. http://dx.doi.org/10.1046/j.1365-2117.2002.00176.x.
Stoner, J.S., St-Onge, G., 2007. Magnetic stratigraphy: reversals, excursions, paleo intensity and secular variation. In: Hillaire-Marcel, C., de Vernal, A. (Eds.), Proxies in Late Cenozoic Paleoceanography; Developments in Marine Geology. Elsevier, pp. 99–137.
Taira, A., 1989. Magnetic fabrics and depositional processes. In: Taira, A., Masuda, F. (Eds.), Sedimentary Facies in the Active Plate Margin. Terra Scientific Publishing Company, Tokyo, pp. 43–77.
Tauxe, L., 1998. Paleomagnetic principles and practice. Modern Approaches in Geophysics. Kluwer Academic Publishers http://dx.doi.org/10.1029/00EO00122.
Taylor, B., Weiss, J.R., Goodliffe, A.M., Sachpazi, M., Laigle, M., Hirn, A., 2011. The structures, stratigraphy and evolution of the Gulf of Corinth Rift, Greece. Geophys. J. Int. 185, 1189–1219. http://dx.doi.org/10.1111/j.1365-246X.2011.05014.x.
Tsimplis, M., 1995. Tidal oscillations in the Aegean and Ionian seas. Estuar. Coast. Shelf Sci. 39, 201–208.
Van Welden, A., 2007. Enregistrements sédimentaires imbriqués d'une activité sismique et de changements paléo-environnementaux. Etude comparée de différents sites : Golfe de Corinthe (Grèce), Lac de Shkodra (Alabanie/Montenegro), Golfe de Cariaco (Vénézuela) (PhD Thesis) University of Savoie.
Verdicchio, G., Trincardi, F., 2008a. Shallow-water contourites. Developments in Sedimentology, Developments in Sedimentology. Elsevier, pp. 409–433 http://dx.doi.org/10.1016/S0070-4571(08)10020-6.
Verdicchio, G., Trincardi, F., 2008b. Mediterranean shelf-edge muddy contourites: examples from the Gela and South Adriatic basins. Geo-Mar. Lett. 28, 137–151. http://dx.doi.org/10.1007/s00367-007-0096-9.

Further Reading

Sakellariou, D., Lykousis, V., Papanikolaou, D., 2001. Active faulting in the Gulf of Corinth, Greece. Rapp. Comm. Int. Mer Médit. 36.